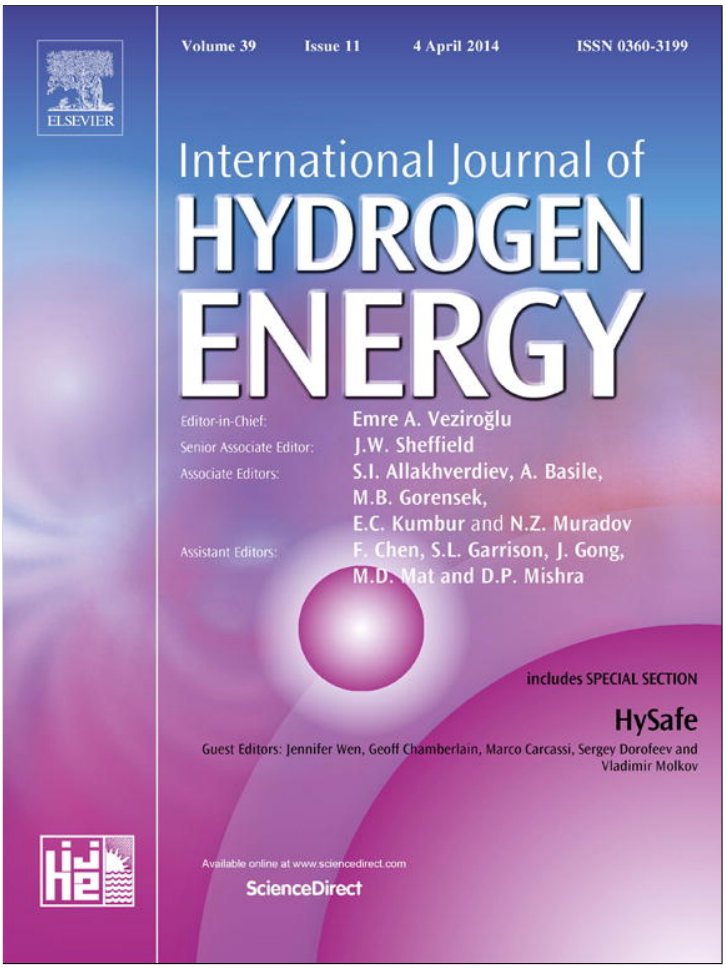

INTERNATIONAL JOURNAL OF HYDROGEN ENERGY 39 (2014) 5818–5851

Available online at www.sciencedirect.com

ScienceDirect

journal homepage: www.elsevier.com/locate/he

Review

Metal hydride hydrogen compressors: A review☆

M.V. Lototskyy [a,*], V.A. Yartys [b,c,**], B.G. Pollet [a], R.C. Bowman Jr. [d]

[a] HySA Systems Competence Centre, South African Institute for Advanced Materials Chemistry, University of the Western Cape, Private Bag X17, Bellville 7535, South Africa
[b] Institute for Energy Technology, P.O. Box 40, Kjeller NO-2027, Norway
[c] Norwegian University of Science and Technology, Trondheim NO-7491, Norway
[d] Oak Ridge National Laboratory, P.O. Box 2008, Oak Ridge, TN 37831, USA

ARTICLE INFO

Article history:
Received 13 December 2013
Received in revised form
23 January 2014
Accepted 24 January 2014
Available online 26 February 2014

Keywords:
Metal hydrides
Hydrogen compression
Energy efficiency
Heat utilisation

ABSTRACT

Metal hydride (MH) thermal sorption compression is an efficient and reliable method allowing a conversion of energy from heat into a compressed hydrogen gas. The most important component of such a thermal engine – the metal hydride material itself – should possess several material features in order to achieve an efficient performance in the hydrogen compression. Apart from the hydrogen storage characteristics important for every solid H storage material (e.g. gravimetric and volumetric efficiency of H storage, hydrogen sorption kinetics and effective thermal conductivity), the thermodynamics of the metal–hydrogen systems is of primary importance resulting in a temperature dependence of the absorption/desorption pressures). Several specific features should be optimised to govern the performance of the MH-compressors including synchronisation of the pressure plateaus for multi-stage compressors, reduction of slope of the isotherms and hysteresis, increase of cycling stability and life time, together with challenges in system design associated with volume expansion of the metal matrix during the hydrogenation.

The present review summarises numerous papers and patent literature dealing with MH hydrogen compression technology. The review considers (a) fundamental aspects of materials development with a focus on structure and phase equilibria in the metal –hydrogen systems suitable for the hydrogen compression; and (b) applied aspects, including their consideration from the applied thermodynamic viewpoint, system design features and performances of the metal hydride compressors and major applications.

* *Corresponding author*. Tel.: +27 21 959 9314; fax: +27 21 959 9312.
** *Corresponding author*. Institute for Energy Technology, P.O. Box 40, Kjeller NO-2027, Norway. Tel.: +47 63 80 64 53; fax: +47 73 81 29 05.
E-mail addresses: mvlot@hysasystems.org, mlototskyy@uwc.ac.za (M.V. Lototskyy), volodymyr.yartys@ife.no (V.A. Yartys).

0360-3199/$ – see front matter
http://dx.doi.org/10.1016/j.ijhydene.2014.01.158

1. Introduction

Metal Hydride (MH) hydrogen compression utilises a reversible heat-driven interaction of a hydride-forming metal, alloy or intermetallic compound with hydrogen gas to form MH and is considered as a promising application for hydrogen energy systems. This technology, which initially arose in early 1970s, still offers a good alternative to both conventional (mechanical) and newly developed (electrochemical, ionic liquid pistons) methods of hydrogen compression. The advantages of MH compression include simplicity in design and operation, absence of moving parts, compactness, safety and reliability, and the possibility to consume waste industrial heat instead of electricity.

Results of more than 40 years of R&D activities in the development of MH hydrogen compression have been reported in numerous original research papers, patents, reports and conference presentations. However, few review articles on the topic are available. A brief review on the principle of H_2 compression using MH, related R&D within the field and their own feasibility studies of MH H_2 compression was published by Lynch et al. in 1984 [1]. A detailed consideration of the related MH-based thermodynamic engines (heat pumps) was presented by Dantzer and Orgaz in three review papers [2–4], 1986–1987. A general approach to the development of the MH hydrogen compressors for various applications based on thermodynamic analysis was considered by Solovey in 1988 [5]. Rather comprehensive reviews of MH compressors and heat pumps were published as sections of general review papers on applications of metal hydrides, by Sandrock in 1994 [6] and Dantzer in 1997 [7]. Bowman has reviewed the development of metal hydride compressors for the liquefaction of hydrogen via the Joule–Thomson process [8,9]. Status of the development of metal hydride based heating and cooling systems was summarised in a paper by Muthukumar and Groll [10] in 2010.

The present review summarises the state of the art of the MH hydrogen compression technology, by considering and discussing the relevant data in materials and systems development, analysis of design features and performances of the MH compressors, and their applications. For the sake of better understanding of the processes taking place in the MH hydrogen compressors, the first section of the review presents relevant fundamental aspects focused on the consideration of the suitable hydride forming materials for hydrogen compressors.

2. Metal–hydrogen systems from a fundamental viewpoint

Applications of metal hydrides, including hydrogen compression, utilise a reversible heat-driven interaction of a hydride-forming metal/alloy, or intermetallic compound (IMC) with hydrogen gas, to form a metal hydride:

$$M(s) + x/2\ H_2(g) \underset{\text{desorption}}{\overset{\text{absorption}}{\rightleftharpoons}} MH_x(s) + Q; \quad (1)$$

where M is a metal/alloy (e.g., V or a BCC solid solution based upon it), or an IMC ($LaNi_5$, TiFe, etc.); (s) and (g) relate to the solid and gas phases, respectively. The direct interaction, an exothermic formation of the metal hydride/hydrogen absorption, is accompanied by a release of heat, Q. The reverse process, endothermic hydride decomposition/hydrogen desorption, requires supply of approximately the same amount of heat.

The following gas phase applications of metal hydrides use specific features of the Reaction (1) [6–12]:

- Compact and efficient hydrogen storage is due to a very high, about 100 g_H/L, volumetric density of atomic hydrogen accommodated in the crystal structure of the MH metal matrix. At ambient temperatures the equilibrium of the Reaction (1) can often take place at modest, ≤1–10 bar hydrogen pressures. Thus, hydrogen storage using MH is intrinsically safe and benefits from avoiding use of compressed hydrogen gas and energy inefficient and potentially unsafe liquid H_2. Endothermic reverse process of dehydrogenation according to the Reaction (1) decreases temperature of the MH leading to decreased rates of H_2 evolution; this, in turn, is an additional safety feature of use of the MH, allowing to avoid accidents even in case of rupture of the hydrogen storage containment.
- Simple and efficient pressure/temperature swing absorption–desorption systems. This allows not only to control hydrogen pressure by changing temperature, but, furthermore opens possibilities for hydrogen separation and purification (including isotope separation) due to the high selectivity of the Reaction (1).
- Reversibility and significant heat effects (≥20 kJ/mol H_2) of the Reaction (1) make it possible to realise numerous energy conversion applications of MH. This includes first of all thermally driven hydrogen compression and heat management.

The process performances, especially for the latter applications considered in the present review, are strongly dependent on the intrinsic features of the Reaction (1) including its thermodynamic and kinetic characteristics (the macro-kinetic parameters involving heat-and-mass transfer issues are also very important), as well as composition, structure and morphology of the solid phases (M, MH_x) involved in the process. These features, mainly related to fundamental aspects of MH materials science, are considered in the current section.

2.1. Phase equilibria in the metal–hydrogen systems

Equilibrium of the Reaction (1) is characterised by an interrelation between hydrogen pressure (P), concentration of hydrogen in the solid phase (C) and temperature (T). This relation (PCT-diagram) is the characteristic feature of a specific hydride-forming material determining thermodynamics of its interaction with gaseous hydrogen. At the same time, thermodynamic behaviour of the metal–hydrogen systems has common characteristics, which are similar for different materials [13].

At low hydrogen concentrations ($0 \le C < a$) hydrogen atoms form an interstitial solid solution in the metal matrix (α-

Table 1 – Equilibrium characteristics of the interaction of hydride-forming alloys suitable for H_2 compression with H_2 gas in plateau region. The data are sorted in the ascending order for desorption plateau pressure at T = 25 °C (P_0). The plateau pressures are calculated using Equation (2); the lower (P_L) and higher (P_H) values correspond to the lower (T_L) and higher (T_H) temperatures, respectively, as reported in the original works.

# [a]	Alloy	$-\Delta S^0$ [J/(mol H_2 K)]	$-\Delta H^0$ [kJ/mol H_2]	Temperature range [°C]		Pressure [atm]			Ref.
				T_L	T_H	P_0	P_L	P_H	
1 (A)	$V_{75}Ti_{17.5}Zr_{7.5}$	145.1	52.98	30	120	0.02	0.03	3.47	[15]
2 (B)	$MmNi_{4.8}Al_{0.2}$	111.3	37.20	50	150	0.02	0.63	16.66	[16],[b]
3 (B)	$LaNi_{4.7}Sn_{0.3}$	112.6	36.51	25	80	0.31	0.31	3.03	[17]
4 (A)	$V_{75}Ti_{10}Zr_{7.5}Cr_{7.5}$	132.3	42.23	30	120	0.32	0.43	19.90	[15]
5 (B)	$LaNi_{4.8}Sn_{0.2}$	104.3	32.83	20	90	0.50	0.40	5.32	[18],[b]
		105.0	32.80	0	240	0.55	0.16	139.9	[19]
6 (B)	$Mm_{0.5}La_{0.5}Ni_{4.7}Sn_{0.3}$	111.2	33.80	25	80	0.77	0.77	6.44	[17]
7 (B)	$LaNi_{4.8}Al_{0.2}$	101.6	30.40	50	150	0.96	2.47	35.84	[16],[b]
8 (B)	$LaNi_5$	110.0	31.80	25	200	1.49	1.49	171.9	[20,21][b]
9 (B)	$MmNi_{4.7}Fe_{0.3}$	87.4	25.00	20	102	1.53	1.29	12.14	[22],[b]
10 (A)	$V_{0.85}Ti_{0.1}Fe_{0.05}$	148.0	42.90	−20	100	1.64	0.08	53.14	[20,23][b]
11 (C)	$TiFe_{0.9}Mn_{0.1}$	107.7	29.70	0	100	2.64	0.88	29.39	[20,24][b]
12 (B)	$La_{0.85}Ce_{0.15}Ni_5$	91.28	24.30	10	110	3.24	1.93	28.50	[b,c]
13 (B)	$MmNi_{4.7}Al_{0.3}$	107.8	28.88	20	90	3.73	3.05	29.98	[18]
14 (A)	$V_{92.5}Zr_{7.5}$	147.0	40.32	30	60	4.11	5.38	22.71	[15]
15 (B)	$La_{0.2}Y_{0.8}Ni_{4.6}Mn_{0.4}$	105.3	27.10	20	90	5.62	4.67	39.78	[25]
16 (D)	$Zr_{0.7}Ti_{0.3}Mn_2$ [d]	85.0	21.00	30	150	5.77	6.63	70.41	[26],[b]
17 (D)	$Ti_{0.9}Zr_{0.1}Mn_{1.4}Cr_{0.35}V_{0.2}Fe_{0.05}$ [e]	106.9	25.89	25	100	11.17	11.17	91.14	[27]
18 (B)	$MmNi_{4.15}Fe_{0.85}$	105.4	25.00	25	200	11.36	11.36	502.8	[20,24][b]
19 (B)	$La_{0.4}Ce_{0.4}Ca_{0.2}Ni_5$	115.3	28.20	15	100	12.08	8.14	118.9	[28]
20 (D)	$Ti_{0.8}Zr_{0.2}CrMn$	108.6	24.60	−20	50	23.06	3.95	49.69	[20],[b]
21 (B)	$Mm_{1-x}Ca_xNi_{5-y}Al_y$ [e]	103.0	22.85	5	90	23.82	12.28	124.0	[29]
22 (B)	$Ca_{0.2}Mm_{0.8}Ni_5$	109.5	24.50	0	100	26.75	10.83	195.0	[20,24][b]
23 (D)	$Zr_{0.8}Ti_{0.2}FeNi_{0.8}V_{0.2}$	118.3	26.80	20	90	30.49	25.35	211.1	[30],[b]
24 (D)	$Ti_{0.77}Zr_{0.3}Cr_{0.85}Fe_{0.7}Mn_{0.25}Ni_{0.2}Cu_{0.03}$	93.66	19.26	20	110	32.98	28.88	184.8	[c]
25 (D)	$TiCr_{1.9}Mo_{0.01}$	113.0	24.80	−50	90	36.11	1.25	216.4	[30]
26 (D)	$TiCr_{1.9}$	122.0	26.19	−100	30	60.77	0.03	72.34	[31],[b]
27 (D)	$ZrFe_{1.8}Cr_{0.2}$	109.0	22.30	20	90	61.19	52.49	306.2	[30]
28 (D)	$(Ti_{0.97}Zr_{0.03})_{1.1}Cr_{1.6}Mn_{0.4}$	115.0	23.40	10	99	80.80	49.00	527.9	[32]
29 (D)	$TiCr_{1.5}Mn_{0.25}Fe_{0.25}$ [e]	101.6	19.32	−10	165	83.61	29.65	1009	[27]
30 (D)	$TiCr_{1.5}Mn_{0.2}Fe_{0.3}$ [e]	101.0	18.32	−10	148	116.4	43.57	1008	[27]
31 (D)	TiCrMn	106.0	19.60	−60	100	126.8	5.42	621.2	[34],[b]
32 (D)	$ZrFe_{1.8}Ni_{0.2}$	119.7	21.50	20	90	306.0	264.0	1445	[30]
33 (D)	$Ti_{0.86}Mo_{0.14}Cr_{1.9}$	117.0	17.20	−50	90	1253	121.7	4340	[30]

[a] Type of the alloy is specified in brackets as BCC-V solid solution (A); AB_5- (B), AB- (C) and AB_2-type (D) IMC's.
[b] The data are also available at the US DoE hydrogen storage materials database, http://hydrogenmaterialssearch.govtools.us; section "Hydride Information Center (Hydpark)".
[c] Previously unpublished experimental data by the authors of this review (ML, VY).
[d] Dynamic PCT experiments.
[e] ΔS^0 fitted by ML to agree with the reported T–P conditions.

phase) with $C(H) \sim \sqrt{P(H_2)}$ according to a Henry–Sieverts law. When the value of C exceeds concentration of the saturated solid solution (a), precipitation of the hydride (β-phase with hydrogen concentration $b > a$) occurs, and the system exhibits features of first order phase transition taking place at a constant hydrogen pressure, $P = P_P$ ($a \le C \le b$). This pressure is called as plateau pressure in the diagrams of the metal–hydrogen systems. Further increase in hydrogen concentration is again accompanied by the pressure increase corresponding to the formation of H solid solution in the β-phase. When the concentration approaches a certain maximum value ($C \to C_{max}$) corresponding to the maximum hydrogen storage capacity of the material, or the number of interstitial sites available for the insertion of H atoms, the equilibrium pressure exhibits an asymptotic increase, $P \to \infty$.

The plateau width, ($b-a$), is often considered as a reversible hydrogen capacity of the material, and the equilibrium of Reaction (1) in the plateau region is described by van't Hoff equation:

$$\ln\left(\frac{P_P}{P^0}\right) = -\frac{\Delta S^0}{R} + \frac{\Delta H^0}{RT}; \quad (2)$$

where $P^0 = 1$ atm $= 1.013$ bar,[1] ΔS^0 and ΔH^0 are the standard entropy and enthalpy of hydride formation respectively, R is the gas constant.

[1] Often, when presenting Equation (2) in the literature, P^0 is omitted. Note that in this case the P_P units are atmospheres, since the Equation (2) refers to a standard state at $P = 1$ atm; $T = 25$ °C.

The values of plateau pressures, P_P, at a given temperature are thus dependent on ΔS^0 and ΔH^0 which are individual properties of the material. For various hydride forming alloys and IMC's, ΔS^0 varies insignificantly around -111 ± 14 J/(mol H_2 K), see Table 1; that value is close for different systems as this is the change of entropy of gaseous H_2 during the Reaction (1) originating from the main/configurational contribution (about -130 J/(mol H_2 K)) to the entropy from dissociation of H_2. Consequently, the plateau pressure will be mainly determined by the reaction enthalpy, ΔH^0, which widely varies for different metals and is a measure of the average strength of the M–H bond in MH_x [14]. The latter is strongly dependent on the composition and crystal structure of the parent metallic material, including type of its components (as regards to their affinity to hydrogen), their stoichiometry and interaction energy in the alloy or IMC, type/surrounding and size of the interstitial sites in the metal matrix available for the insertion of the H atoms.

Since P_P increases exponentially with temperature, the low-temperature H absorption at $P_{H_2} > P_P(T_L) = P_L$ takes place at a lower hydrogen pressure, and the high-temperature H desorption ($P_{H_2} < P_P(T_H) = P_H$) occurs at a higher pressure, similar to the suction and discharge processes in a mechanical compressor.

Table 1 presents the equilibrium properties of hydrogen interaction with some hydride-forming alloys and IMC's suitable for hydrogen compression applications. Van't Hoff plots for some of these materials are presented in Fig. 1; typical requirements for the H_2 compression ($P = 1$–400 atm, $T = 25$–150 °C) are shown as a rectangular area.

It can be seen that, depending of the type (A–D) and composition of the hydride-forming material, the equilibrium hydrogen pressures vary in a very broad range, from below 1 bar to exceeding 1 kbar at room temperature. Most of the lower-pressure H_2 compression alloys ($P_H < 200$ bar at $T_H < 150$ °C) belong to the AB_5-type intermetallic compounds (group B in Table 1) while significantly higher, >1 kbar, hydrogen pressures can be generated using AB_2-type IMC's (group D).

As it can be seen from Fig. 2, hydrogen compression ratio (P_H/P_L) achieved using MH in the temperature range from $T_L \sim 25$ °C to $T_H = 100$–150 °C varies in the range 10–50 at $P_H = 100$ atm. The value of P_H/P_L has a tendency to become smaller when P_H increases, but remains quite high (5–10) even for the H_2 discharge pressures ≥1 kbar.

It has to be noted that the presented above hydrogen compression performances calculated on the basis of van't Hoff Equation (2) are only rough estimates which significantly deviate from real characteristics of metal hydride materials, even being considered only from thermodynamic point of view.

The major factor affecting hydrogen compression efficiency of the MH materials is the plateau slope. In a multicomponent hydride-forming IMC's (e.g., AB_n) the sloping plateaux are originated from compositional fluctuations due to the presence of impurities randomly substituting A- and/or B-component, or because of fluctuations of the stoichiometry ($AB_{n\pm x}$) within the homogeneity region [35]. The quantification of this phenomenon by introducing statistical (as a rule, Gaussian) distribution of P_P was first suggested by Larsen and Livesay [36] and further developed by Fujitani et al. [37], Lototsky, Yartys et al. [38,39], Park et al. [40].

In addition to operating pressure–temperature ranges, an important parameter of MH material for hydrogen compression is the process productivity. The simplest approach for its estimation assumes the productivity of H_2 compression cycle (per unit of weight or per number of the metal atoms) as (b–a), i.e. plateau width, where the values of b and a are available. The problem of this approach is that both a and b are temperature-dependent, and the plateau width decreases with increase of the temperature. Furthermore, at a critical temperature, T_C, the plateau degenerates to an inflection

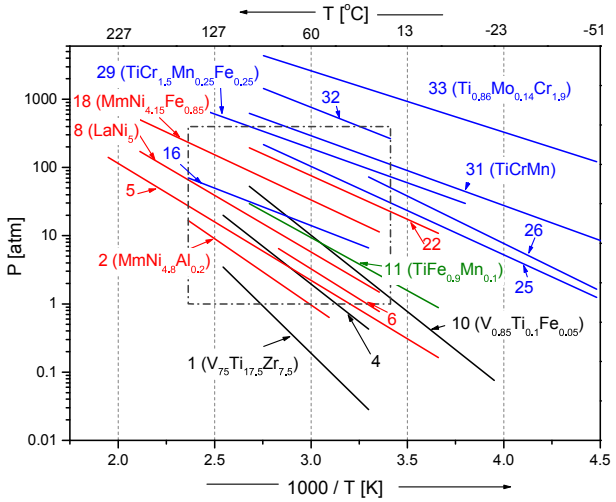

Fig. 1 – Van't Hoff plots for selected hydride-forming alloys suitable for H_2 compression. Plot numbers correspond to the numbers of alloys in Table 1; plot colours correspond to the types of the hydride-forming alloys (A – black, B – red, C – olive, D – blue). Rectangular area limited by dash-dot line shows target requirements for H_2 compression: $P = 1$–400 atm, $T = 25$–150 °C. (For interpretation of the references to colour in this figure legend, the reader is referred to the web version of this article.)

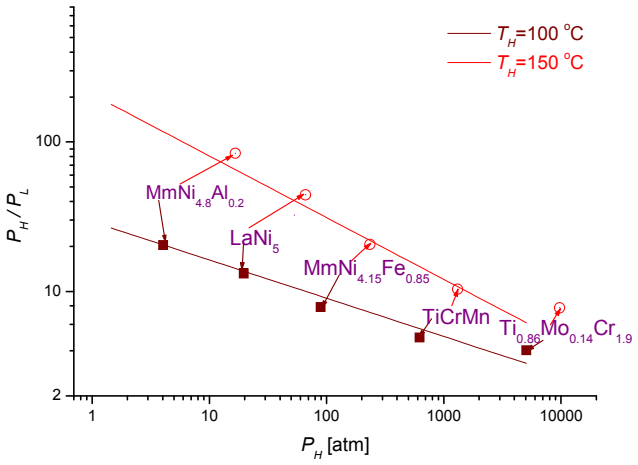

Fig. 2 – Dependencies of hydrogen compression ratio at $T_L = 25$ °C for selected hydride-forming alloys (Table 1).

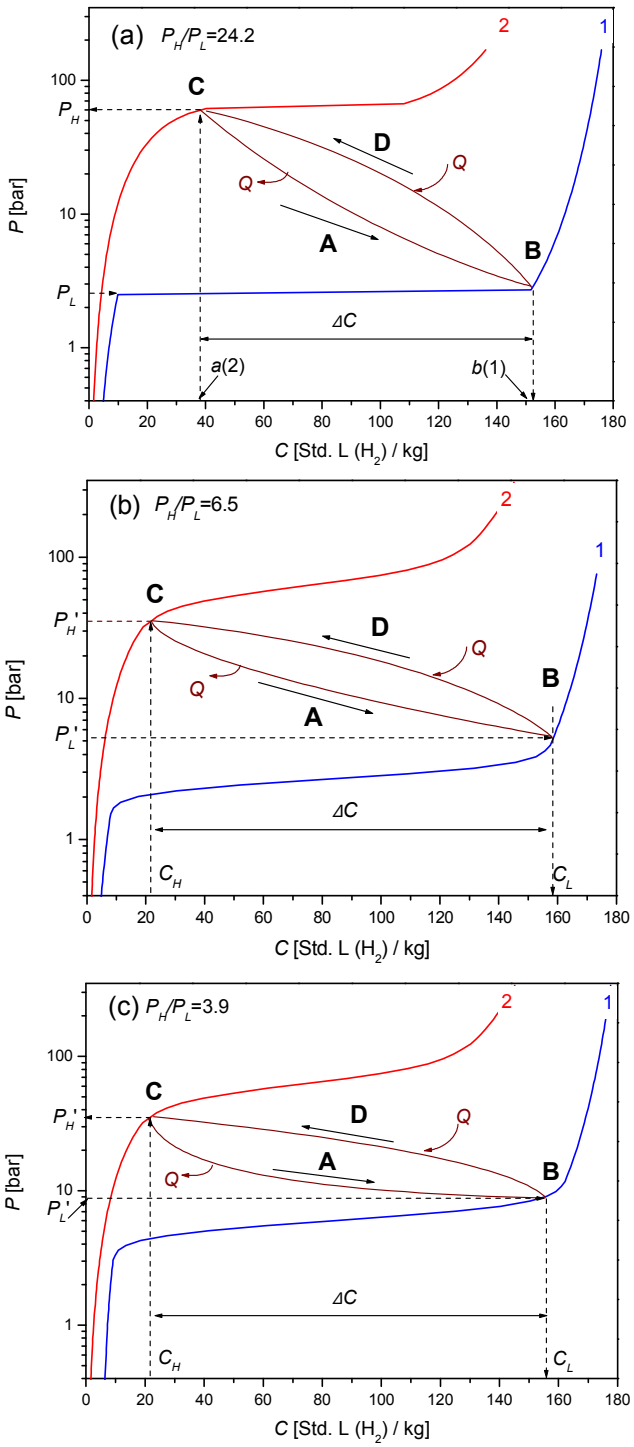

Fig. 3 – Pressure–composition isotherms at T_L = 20 °C (1) and T_H = 150 °C (2) for H–$La_{0.85}Ce_{0.15}Ni_5$ system illustrating thermally-driven hydrogen compression using MH: (a) – idealised (flat plateaux, desorption isotherms), (b) – idealised (sloping plateaux, desorption isotherms), (c) – real (sloping plateaux, absorption isotherm at T_L, desorption isotherm at T_H).

point, and at $T > T_C$, the pressure–composition isotherms are continually sloping [14]. Hence, for a realistic estimation of the hydrogen compression productivity it is necessary to know temperature dependencies of a and b, or to have a quantitative information about phase diagram of the hydrogen–metal system. The corresponding approach for the modelling of PCT diagrams using statistical and thermodynamic features was suggested by Lacher for H–Pd system already in 1937 [41] and further developed by Kierstead [42], Brodowsky et al. [33], Beeri et al. [34], Lototsky, Yartys et al. [39].

Finally, hydrogen compression performances of the real MH systems are significantly affected by hysteresis, as the values of plateau pressures for hydrogen absorption/hydrogenation are higher than the ones for hydrogen desorption/dehydrogenation. Hysteresis is caused by stresses which appear in the course of growth of MH nuclei inside the matrix of the MH alloy having lower molar volume. The thermodynamic aspects of hysteresis were discussed in detail in a number of publications (see, e.g. Refs. [13,43,44]). The influence of hysteresis on the performance of MH hydrogen compressors will be discussed in section 3.2.

Taking into account the features of phase equilibria in the real metal–hydrogen systems described above, we can illustrate the process of thermally-driven hydrogen compression using MH by the scheme shown in Fig. 3.[2] Hydrogen is absorbed in the MH at a lower temperature, T_L, following the hydrogen absorption isotherm at T_L (1); the process is accompanied by a release of heat, $Q \approx |\Delta H^0|$. The absorption is carried out at a lower pressure, so the system approaches equilibrium which corresponds to the point B on the isotherm (1). The corresponding value of hydrogen concentration (C_L) is strongly dependent on the hydrogen pressure and, generally, it is not equal to the lower limit, b(1) (see Fig. 3(a)), of hydrogen concentration in β-hydride at T_L.

Further heating of the system to a higher temperature, T_H, results in the hydrogen desorption from MH which follows the hydrogen desorption isotherm at T_H (2) and requires absorption of heat, Q. When the desorbed hydrogen is released at a higher pressure, the system equilibrium corresponds to the point C on the desorption isotherm (2). Similarly, hydrogen concentration (C_H) in this point depends on the hydrogen desorption pressure and may not be equal to hydrogen concentration, a(2) (see Fig. 3(a)), in the saturated α-solid solution at T_H.

In the real systems, due to sloping plateau (Fig. 3(b)) and hysteresis (Fig. 3(c)), hydrogen compression in the same temperature range (from T_L to T_H corresponding to isotherms 1 and 2, respectively) will require higher suction pressures ($P_L' > P_L$) and lower discharge pressures ($P_H' < P_H$) than the corresponding values calculated by Van't Hoff Equation (2) using ΔS^0 and ΔH^0 reference data (Table 1; usually provided for desorption). Accordingly, the compression ratio, P_H'/P_L', will be lower than the P_H/P_L estimation based on the ideal plateau behaviour, Fig. 3(a).

Hydrogen compression from P_L' to P_H' carried out in the temperature range from T_L to T_H is represented by a cyclic process involving hydrogen absorption (A) and hydrogen desorption (D) between points B and C on the isotherms 1 (H absorption) and 2 (H desorption), respectively.

[2] Figs. 3 and 4 are made on the basis of the unpublished experimental PCT data for $La_{0.85}Ce_{0.15}Ni_5$ further processed by the model of Lototsky, Yartys et al. [39].

Independent of specific paths B → C (D) and C → B (A), the amount of hydrogen taking part in the compression cycle (or cycle productivity of the process) will be equal to the change of hydrogen concentration in the solid (ΔC). For the specific MH material this value will be strongly dependent on the process conditions (T_L, T_H, P_L' and P_H'; Fig. 3(c)). The described evaluations are based on maintaining of both T_L and T_H, which requires enhancements of the heat transfer [45] due to the poor thermal conductivity of hydride powders (see Sections 2.2 and 3.3).

Fig. 4 presents calculated values of ΔC for $La_{0.85}Ce_{0.15}Ni_5$ at $T_L = 20$ °C and $T_H = 150$ °C. As it can be seen, at the suction pressure (P_L') above the midpoint of the sloping plateau of the H absorption isotherm, the hydrogen compression productivity significantly increases. Increase of the discharge pressure (P_H') results in the significant loss of the productivity. However, if the suction pressure is high enough (that corresponds to β-region of the H absorption isotherm (1), see Fig. 3), very high discharge pressures can be generated with the productivity about 20% of the reversible hydrogen capacity of the material at T_L. This effect has its origin in (i) decrease of the lower limit, *b*, of hydrogen concentration in β-hydride with increasing the temperature, and (ii) contribution of the dissolved hydrogen additionally released from the β-hydride. Increase of T_H will result in further increase of the discharge pressure with no significant changes in productivity, due to the lowering of the concentration, *a*, of the saturated α-solid solution.

The feasibility of generating high H_2 pressures using quite stable MH was mentioned by Golubkov and Yuhimchuk [46] who reported about compression of hydrogen isotopes to 57 bar ($TiH_2/T_H = 700$ °C), 85 bar (UH_3/700 °C) and 700 bar (VH_2/250 °C).

In summary, selection of the MH materials able to provide required H_2 compression from P_L to P_H in the available temperature range (T_L to T_H) can be achieved by analysing dependence of thermodynamic properties (enthalpy and entropy) of hydrogenation/dehydrogenation, on the alloy composition. More accurate thermodynamic estimations of hydrogen compression performances of MH materials, including suction (P_L') and discharge (P_H') pressures at cooling (T_L) and heating (T_H) temperatures, compression ratio (P_H'/P_L') and the process cycle productivity (ΔC), are possible when considering the complete isotherms of hydrogen absorption at T_L and hydrogen desorption at T_H, taking into account plateau slope, hysteresis and features of H–M phase diagram. This assessment can be done by the fitting the available experimental PCT data using suitable models of phase equilibria in metal–hydrogen systems.

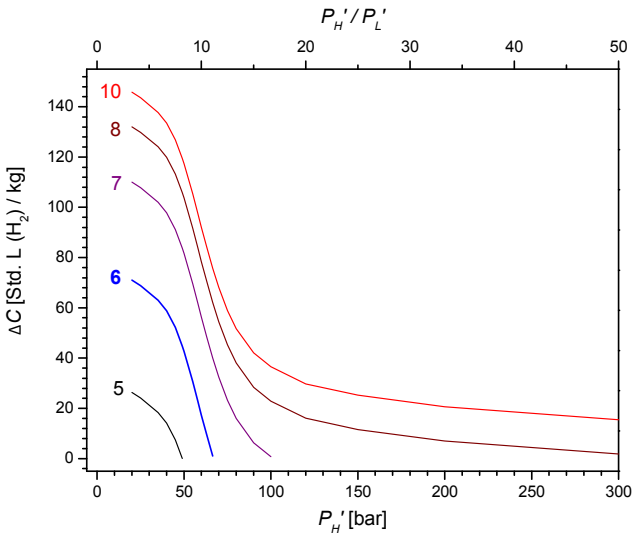

Fig. 4 – Dependence of H_2 compression cycle productivity, ΔC, for the H–$La_{0.85}Ce_{0.15}Ni_5$ system (Fig. 3) on the H_2 desorption pressure, P_H', at $T_H = 150$ °C. Curve numbering corresponds to the H_2 absorption pressure, P_L' [bar], at $T_L = 20$ °C. The value $P_L' = 6$ bar corresponds to the plateau midpoint.

2.2. *H sorption/desorption kinetics*

Though cycle productivity of H_2 compression using MH can be determined from the thermodynamic considerations (see previous section), the duration of the hydrogen absorption–desorption cycle and, correspondingly, dynamic performances of MH hydrogen compressors depend on the rates of the direct and reverse processes of Reaction (1), i.e. on kinetics of hydrogen absorption and desorption which can vary significantly from alloy to alloy. Because many intermetallic hydrides exhibit rather fast intrinsic hydrogenation–dehydrogenation kinetics, the rates of H absorption and desorption for the MH storage materials are generally more often limited by heat transfer [45,47]. In some cases, e.g. operation at low temperatures, or in presence of gaseous impurities in hydrogen gas, kinetic factors may become decisive [48]. Thus, heat-and-mass transfer modelling of H_2 charge/discharge flow rates in the MH should incorporate a reliable and verified kinetic expression of the rates of H uptake and release [49,50].

Kinetics and mechanism of hydrogen–metal interaction were analysed in numerous original research papers and review publications (see, e.g. Refs. [49,51]). The interrelation between kinetics and heat transfer determining the eventual rates of H_2 absorption and desorption in various reactors was first considered by Goodell [47]. He concluded that, due to the very fast isothermal H_2 absorption (estimated time of 75% hydrogenation for $LaNi_5$ at $P_{H_2} = 2P_P$ and $T = 25$ °C equals to just 0.5 s) and poor effective thermal conductivity of the MH powder (~1 W/(m K)), the system is quickly self-heated and approaches equilibrium elevated temperature conditions; these can be calculated by solving the van't Hoff Equation (2) taking plateau pressure, P_P, as the actual H_2 pressure. Further H_2 absorption or desorption is limited by the rate of cooling or heating of the MH. Consequently, the most important kinetic aspect in the dynamic behaviour of the MH reactors is hydrogen absorption–desorption rate at near-equilibrium conditions. As it was shown by Førde, Yartys et al. in Ref. [49], a good approximation of the reaction kinetics in this case can be achieved by using Avrami–Erofeev equation:

$$X = 1 - \exp\left[-(K_r t)^n\right]; \quad (3)$$

where *X* is the reacted fraction, K_r is the rate constant, *t* is time, and *n* is integer or half-integer whose value (0.5…4)

depends on the reaction mechanism. The reaction fraction is defined as:

$$X \equiv \frac{C_H - C_1}{C_2 - C_1}; \quad (4)$$

where C_H is the actual hydrogen concentration; C_1 and C_2 is the hydrogen concentrations at the beginning and end of the reaction, respectively.

The value of the rate constant can be presented as a product of the pressure-defined driving force of the process, $K(P)$, and Arrhenius-like pressure independent term:

$$K_r = K(P) \cdot K_0 \exp\left(-\frac{E_a}{RT}\right) \quad (5)$$

where E_a is activation energy.

Note that the pressure driving force, $K(P)$, depends on the deviation of the actual hydrogen pressure from the equilibrium one (typical dependencies for the various reaction mechanisms, e.g. $K(P) = \ln(P_{eq}/P)$ for the desorption, are reviewed in Ref. [49]), and the reaction rates at the given pressure–temperature conditions will be dependent on both kinetic parameters and PCT characteristics of the hydrogen–metal system. This approach is used in the heat-and-mass transfer modelling of the MH reactors for hydrogen compression (section 3.3).

2.3. *Materials challenges and their solution*

Hydrogen compression applications pose the following requirement to MH materials [11,48]:

- Tuneable PCT properties allowing to achieve required hydrogen compression ratio (P_L to P_H) in the available temperature range (T_L to T_H);
- High reversible H storage capacity to minimise the amount of MH and to reduce the energy consumption and the heat losses associated with thermal swings;
- Fast kinetics of hydrogen exchange to achieve higher productivities;
- Low plateau slope of the H absorption and desorption isotherms;
- Low hysteresis, P_A/P_D;
- Cycle stability when operating at high temperatures and H_2 pressures;
- Tolerance of H sorption performances to the impurities in H_2;
- Scaleability of the synthesis of MH alloys and their hydrides, and affordable costs.

The following section briefly describes challenges appearing in the course of the development of MH materials for hydrogen compression and reviews the possible ways of their solution.

2.3.1. *Tuning of the thermodynamic properties*

As it was shown in section 2.1, hydrides of the alloys and IMC's form and decompose in a broad range of equilibrium decomposition pressures. Taking into account the non-ideal behaviours reflected in the shape of the pressure–composition isotherms (primarily, plateau slope and hysteresis), the achievable compression ratio at a reasonable cycle productivity/reversible H capacity is low and seldom exceeds 5–10 at $(T_H - T_L) \approx 100$ K, Thus, a multistage compression (see section 3.1) is required to reach higher eventual compression values. The multistage operation approach introduces more strict requirements to the tuneability of the PCT characteristics, since in this case the H desorption isotherm at T_H for the previous stage and H absorption isotherm at T_L for the next stage must be synchronised. The problem of coupling of the MH materials used in the consecutive hydrogen compression stages resembles selection of "high-temperature" and "low-temperature" MH for the heat management applications [3,10]. However, in case of hydrogen compression, special attention has to be paid to the operating pressures, in addition to the thermal properties of the corresponding systems.

Altering of the hydrides stability can be achieved by the variation of the composition of the parent alloys. The existent hydride-forming alloys allow very broad, from −70 to −20 kJ/mol H_2, variation in ΔH^0 that corresponds to the H_2 plateau pressures from millibars to kilobars at room temperature [12]. As applied to the commonly used types of hydride-forming alloys and IMC's, the variation in composition offers the following opportunities described in Table 1 and in Fig. 1.

AB_5-type intermetallics, the most rugged materials for the MH applications, allow variation of the lower/suction pressures from <1 to 20–30 bar at $T_L = 25$ °C, and the higher/discharge pressures from 15–20 to ~200 bar at $T_H = 100$–150 °C. The variations of the thermodynamic stability of the AB_5-based hydrides can be achieved by substitution of lanthanum in $LaNi_5$ by cerium or mischmetal[3] (this lowers the stability and increases the H_2 dissociation pressures), and by substitution of nickel with cobalt, aluminium, manganese, or tin (increasing the stability, and decreasing the H_2 pressures). The AB_5-type IMC's have rather small plateau slope and hysteresis, however, increasing with the increase in cerium/mischmetal, and/or aluminium content [16,52]. Introduction of aluminium also results in decrease of the reversible hydrogen capacity [16]. However, Al substitution significantly enhances the durability of the hydride phase during extended absorption/desorption cycling as has been demonstrated for several AB_5-type alloys [53–56].

Industrial-scale manufacturing of AB_5-type alloys for hydrogen compression, as well as influence of the substituting components (Ce, Co, Al) in $LaNi_5$ on the operating performances of the MH materials has been studied by Baichtok et al. [57]. The application of (La,Ce)Ni_5 for industrial-scale hydrogen compression was reported by Bocharnikov et al. [58].

AB_2-type intermetallics cover much broader range of the operating pressures. The most stable $ZrV_2H_{\sim 4}$ is characterised by thermodynamic parameters of β–α transition as $\Delta S^0 = -88.4$ J/(mol H_2 K) and $\Delta H^0 = -78$ kJ/mol H_2 [59] that

[3] Mischmetal is an alloy of rare earth metals in naturally occurring proportions and is available in two modifications, as a lanthanum mischmetal containing 58.0 wt.% La, 28.6 wt.% Ce, 5.8 wt.% Pr and 7.5 wt.% Nd (produced by Norsk Hydro and used in Ref. [17]), or as a cerium mischmetal containing ~50% cerium and ~25% lanthanum, with the rest divided between neodymium and praseodymium as in Ref. [16].

corresponds to plateau pressure below 10^{-6} mbar at room temperature and just around 3 mbar at $T = 300$ °C. At the same time, hydride of $ZrFe_2$ ($\Delta S^0 = -121$ J/(mol H_2 K); $\Delta H^0 = -21.3$ kJ/mol H_2) has plateau pressure above 300 bar at room temperature. A 20% substitution of Zr by Ti results in further destabilisation of the hydride doubling the plateau pressure (this hydride has, however, a huge hysteresis between the pressures of H absorption and desorption) [30]. Since calculated hydrogenation enthalpy of $TiFe_2$ is around −3.6 kJ/mol H_2 [60] and assuming $\Delta S^0 = -100$ J/(mol H_2 K), this will result in a plateau pressure about 40 kbar at a room temperature. Consequently, in the AB_2-type IMC's the operation at higher hydrogen pressures can be achieved by increasing Ti/Zr ratio and Fe content on the, correspondingly, A- and B-sites. The lowering of the operating pressures is achieved by introducing such B-elements as V and, in a lesser extent, Mn and Cr. The multicomponent AB_2-type hydrides appear to show rather high plateau slopes and a profound hysteresis, especially, for higher Fe contents [27,30]. Furthermore, the AB_2-type alloys are much more sensitive towards poisoning by the traces of active gases, oxygen and water vapour, when present as admixtures in hydrogen gas [48].

Vanadium-based BCC solid solution alloys form another type of the materials suitable for MH hydrogen compression. Vanadium forms two hydrides [61], VH_{1-x} and VH_{2-x} where the transition between the mono- and dihydride is characterised by a reversible hydrogen storage capacity of about 1.9 wt.% H at near-ambient conditions and has a steep temperature dependence of hydrogen equilibrium pressure, associated with unusually high values of entropy and enthalpy of the formation of vanadium dihydride. Due to this reason, the BCC vanadium alloys are attractive candidates for the MH hydrogen compressors [62,63]. Introduction of ≤17.5 at.% of titanium into V alloys allows significant variation of the plateau pressure, approximately from 0.2 to 10 bar at $T = 60$ °C [15]. Similar variations (0.1–20 bar at $T = 80$ °C) were achieved by introduction of 0–7.5 at.% Fe in $(V_{0.9}Ti_{0.1})_{1-x}Fe_x$ [64]. Use of some V-based alloys allows for H_2 compression from 20 bar ($T = 10$ °C) to 150–200 bar ($T = 150$ °C) with reversible H capacity exceeding 150 cm^3/g STP. Minor additives of Zr (7.5 at.%), together with Ti (0–17.5 at.%) and 3*d* transition metals (Cr, Mn, Fe, Co, Ni; up to 7.5 at.%), significantly improve hydrogenation/dehydrogenation kinetics, and the variation of the hydride stability can be achieved by changes in the amount of Ti and the transition metals [15]. The main disadvantage of the usage of BCC-V alloys for H_2 compression is in quite high hysteresis and significant sloping of the H_2 absorption isotherms; increased H_2 absorption plateau pressures lead to significant hysteresis; hysteresis increases during H absorption–desorption cycling [65].

TiFe-based AB-type intermetallics can offer advantage of low costs that makes them an attractive option for the applications of MH. The first heat-driven hydrogen compressor was patented in 1970 by Wiswall and Reilly [66] and used TiFe to compress H_2. However, limited possibilities for the element substitution in TiFe does not allow one to easily vary the stability of its hydrides, as compared to the alloys considered earlier in the review. The other drawbacks of TiFe as a hydrogen compression alloy include presence of two plateaux on the pressure–composition isotherms, high hysteresis, difficulties in activation, and sensitivity to the presence of minor impurities of O_2 and H_2O resulting in a strong deterioration of the hydrogen storage performance. Some improvements can be achieved in the course of alloying of TiFe with Mn or V, addition of deoxidisers (RE metals), as well as variations in the procedures of the material preparation and treatment [48,67].

2.3.2. *Tolerance to the impurities in H_2*

Tolerance of the hydride-forming materials towards impurities in H_2 is a very important property, especially for such "open-ended" MH applications as hydrogen compression. Depending on the alloy–impurity combination, hydrogen storage properties can deteriorate as a result of various types of damages [6,48]:

(1) poisoning: H storage capacity quickly decreases without a concurrent decrease of intrinsic kinetics;
(2) retardation: slowing down of the kinetics of hydrogen exchange without a loss of ultimate storage capacity;
(3) corrosion;
(4) innocuous damage: no surface deterioration takes place, but there can be pseudo-kinetic decreases due to inert gas blanketing.

The mechanism of the deterioration of hydrogen absorption/desorption performances is determined by interaction of the impurity with MH surface (1–3), as well as by slowing down of the gas diffusion (4). Influence of the gas impurities can be quantified by empirical equations; their numerical constants depend on the specific "MH–impurity" combination and have to be determined experimentally [68]. The most important impurities for MH H_2 compression process are oxygen and water vapour which are present in hydrogen produced by electrolysis, or traces of carbon dioxide and monoxide in hydrogen produced from carbonaceous feedstock. Moderate concentrations of these impurities (except of CO) are normally not a serious concern for the AB_5-type alloys, but for titanium-based AB_2- and AB-type ones impurities cause problems [48,67]. Presence of even ppm-scale amounts of CO results in a strong poisoning of even most tolerant to the impurities AB_5-type alloys [67–70].

There are several possibilities in addressing the poisoning problem. Importantly, MH poisoned by the admixtures can be reactivated by vacuum heating [6,48]. Secondly, addition of deoxidisers can help as well. One example of the MH hydrogen compressor [71] implies usage of TiFe doped by 2 wt.% of mischmetal. An efficient method of eliminating poisoning is in a surface modification of hydride-forming alloys, for example, by chemical treatment with a fluorine-containing aqueous solution [72]. The coating of the MH surface by transition metals, particularly with platinum group metals, also improves poisoning tolerance and facilitates reactivation procedure; this method combined with the fluorination enables operation in CO-contaminated hydrogen [69,70]. Reviews on the surface modification techniques increasing the poisoning tolerance of the MH materials were published by Uchida [73] and Lototsky et al. [69]. Introduction of noble metals into MH particles is a part of MH hydrogen storage and compression technologies by Ergenics, Inc. [74]. Surface modification of vanadium, by acidic leaching followed by ball milling with 20 wt.% $LaNi_5$ was also used by Hu et al. [75] for the preparation of the MH material suitable for the second stage of high pressure hydrogen compressor.

Group (representative)	Structure of parent alloy	Structure of hydride	$\Delta V/V_0$ [%]
A (BCC-V)	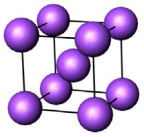	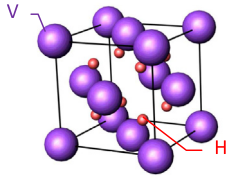	35.5 ($V \rightarrow VH_2$) 30.9 ($V_2H \rightarrow VH_2$)
B ($LaNi_5$)	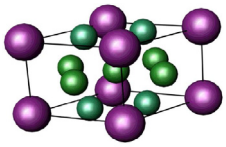	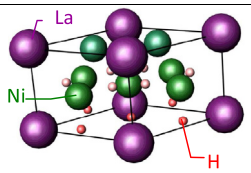	20.4 ($LaNi_5 \rightarrow LaNi_5H_6$)
C ($TiMn_2$)	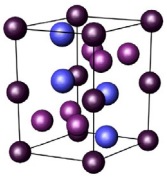	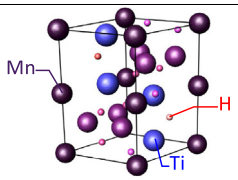	19.6 ($TiMn_2 \rightarrow TiMn_2H_{2.5}$)
D (TiFe)	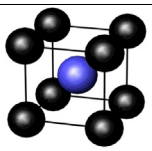	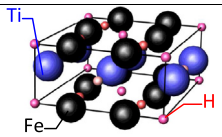	18.3 ($TiFe \rightarrow TiFeH_2$)

Fig. 5 – Crystal structures of parent and hydrogenated alloys used for MH H_2 compression.

2.3.3. *Degradation*

In addition to the cycle stability issues caused by impurity of hydrogen gas, hydrogen storage capacity can be lost during extended cycling in pure H_2 because of the side hydrogenation process dictated by thermodynamics of the metal–hydrogen interactions. A degradation of the reversible H storage capacity is caused by a disproportionation of the intermetallic alloy to form a stable binary hydride [68]. As example, in case of $LaNi_5$, the reversible hydrogen absorption and desorption reaction:

$$LaNi_5 + 3H_2 \rightleftarrows LaNi_5H_6 \quad (6)$$

is less thermodynamically favourable as compared to the irreversible at the same operation conditions disproportionation process:

$$LaNi_5 + H_2 \rightarrow LaH_2 + 5Ni \quad (7)$$

Some intermediate processes take place between Reactions (6) and (7) and include amorphisation, formation of lattice defects and H-trapping sites. For the IMC's enriched with A-component which forms stable binary hydrides (e.g., Y in YNi_2), the disproportionation also results in the formation of intermetallics enriched with the non-hydrided component B (Ni in YNi_5). Because the disproportionation requires diffusion of the metal atoms, it is strongly retarded at lower temperatures, where a reversible formation–decomposition of the intermetallic hydride according to (6) prevails. However, the degradation processes of the type (7) quickly accelerate when temperature and hydrogen pressure increase. That is why the problem of MH intrinsic cyclic stability becomes the most important issue in the course of development of high-pressure MH hydrogen compressors.

The most extended experimental studies of degradation effects during the cycling (up to 90,000 thermal cycles under H_2 pressure; $T = 40–200\ ^\circ C$) were presented in work of M. Groll et al. [76,77]. The reversible H capacities as a function of number of cycles were determined for several AB_5- and AB_2-type alloys. Various investigations (pressure–composition isotherms, TDS, XRD, magnetisation, laser granulometry, SEM/EDS) were performed in order to determine the degradation and regeneration mechanisms involved. The reversible storage capacity of the AB_5 alloys (A = La or Mm; B = Ni, Al, Mn, Co, Sn) decayed during the cycling. This effect is stronger at higher temperatures and pressures. However, the original capacity of the materials could be recovered by heating to ~400–500 °C in vacuum leading to the decomposition of binary hydrides and recombination of intermetallides. Bowman et al. [78] observed nearly full recovery of highly degraded $LaNi_{4.78}Sn_{0.22}$ hydride following a nominal 3 h annealing at ~675 K under circa 1-bar hydrogen pressure. In contrast, the AB_2 alloys (A = Ti, Zr; B = Cr, Mn, Fe, V) showed no degradation after 42,400 cycles [76]. Iosub et al. [79] observed little or nearly isotropic broadening of the X-ray diffraction peaks of AB_2 alloys that they attributed to the reduced defect formation upon

the hydrogen absorption compared to the behaviour of the AB_5 hydrides. This may account for the greater stability exhibited by hydride phases of the AB_2 intermetallics.

The prolonged H sorption–desorption cycling can impair hydrogen sorption properties even for the systems which do not undergo the disproportionation. Indeed, a 20% reduction in H sorption capacity accompanied by increase of hysteresis was observed for vanadium hydride [65] during 1000 absorption–desorption cycles performed between 24 and 135 °C. The most probable reason for that was assumed to be sintering effects accompanied by grain growth and strain relaxation. In chemically related V–Ti–Fe BCC alloys a 40% total decrease of the reversible H capacity was observed after 400 cycles at 10 bar H_2 and 20–600 °C. The cycling was accompanied by a BCC–BCT transition and by the formation of amorphous phase in the MH matrix [80].

During the last decade the material degradation issues for the MH compression materials were studied by Golben and DaCosta [81], Bowman et al. [82–84], Laurencelle et al. [85], Li et al. [86,87]. It was shown that disproportionation resistance of AB_5-type intermetallides increases with increase of the binding energy between the metal atoms, and with introduction of the additives strengthening this interaction (e.g., tin-substituted $LaNi_{5-x}Sn_x$), thus resulting in the improvement of the cycle stability [88].

2.3.4. *Structure and morphology*

Although structural and morphological features of hydride-forming alloys and hydrides are mostly considered as fundamental properties of the MH materials, some of these properties are directly related to the MH compression applications.

Fig. 5 presents the structures of typical hydrogen storage alloys following their classification shown in Table 1. As it can be seen from the last column, the hydrogenation is accompanied by a significant volume increase of the solid materials; the lattice expansion, $\Delta V/V_0$, typically varies from 15 to >30%. Accordingly, the cyclic hydrogen absorption and desorption is accompanied by the periodic changes in the volume of MH material loaded into a container for hydrogen compression.

It is known that insufficiently high filling fraction of the powdered MH material in the MH container results in increase of the "dead space" that significantly decreases H_2 compression productivity, especially, at high discharge pressures [89]. In addition, the increase of the MH packing density is expected to result in the enhancement of the hydride effective thermal conductivity [90]. On the other hand, too high filling density, exceeding 61% of the material density in the hydrogenated state, is detrimental for the operation safety as the lattice expansion during hydrogenation can generate high stresses in the MH bed and, in turn, deform or destroy the container [91].

Fig. 6 illustrates the deformation of a stainless steel vessel following extended absorption–desorption cycling of powder $LaNi_{4.78}Sn_{0.22}$ hydride between ~295 K and 465 K. Thus, the filling of MH material into container for hydrogen compression is always a compromise between achieving the best operation performance and fulfilling safety requirements. The data describing lattice expansion during the hydrogenation ($\Delta V/V_0$) is very important for the optimisation. Since hydrides used for the H_2 compression are unstable at ambient conditions, their structural analysis requires use of *in-situ* neutron

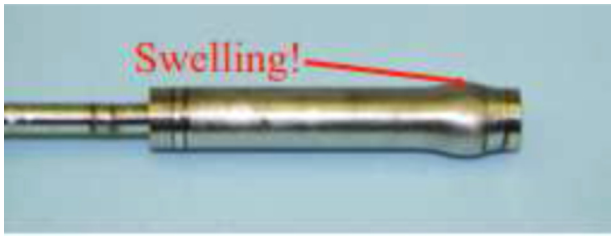

Fig. 6 – Swelling of a 316L stainless steel reactor vessel produced by pressure–temperature cycling of 15 g of $LaNi_{4.78}Sn_{0.22}H_x$ [R.C.Bowman, Jr, previously unpublished].

powder diffraction (NPD) and *in-situ* synchrotron X ray diffraction (SR XRD) allowing to directly monitor phase transformations during the hydrogenation–dehydrogenation. *In-situ* NPD and SR XRD were successfully applied in the detailed studies of a number of hydride systems including ones based on IMC's suitable for high-pressure hydrogen compression [92,93]. Conventional XRD of starting alloys and their hydrides can also be used for the determination of their structural properties, including real (crystal) densities, but its application to probe the unstable hydrides requires their stabilisation by, e.g., exposure to CO, SO_2 [52], or air at liquid nitrogen temperature [94].

Evolution of particle size and shape distribution in the course of cyclic H absorption–desorption processes is a very important factor which determines effective thermal conductivity (ETC) of the powdered MH beds. Recent findings using granular effective medium theory [90] allowed quantifying the interrelation between the morphological features of hydrogenated AB_2-type alloy and heat transfer characteristics of the corresponding MH beds. It opens perspectives for the optimisation of the MH containers for hydrogen compression towards increase of the ETC and, in turn, improvement of their dynamic performances (see also section 3.3.1).

Recently, there were published the data of the detailed experimental study of the influence of cyclic swelling of MH bed on the basis of Ti–V–Cr BCC alloy on the mechanical stresses in the containment, as well as on the changes in MH porosity and their evolution during cyclic hydrogenation/dehydrogenation [95].

3. Applied aspects

3.1. *General layout*

Overviews of the general layouts (Fig. 7) of the MH hydrogen compressors were presented in patent descriptions by the authors of the present review [96,97].

The simplest apparatus realising thermally driven hydrogen compression using MH is shown in Fig. 7(a). Metal hydride material (A) thermally coupled to a heat supply/removal accessory (B) is placed into a pressure container (C) comprising a gas pipeline (D) which allows supply or removal of hydrogen gas to/from MH (A). The gas pipeline (D) can have a built-in filter element (not shown) which provides a uniform hydrogen distribution within the MH bed, and also prevents contamination of gas pipelines with fine powder of the MH.

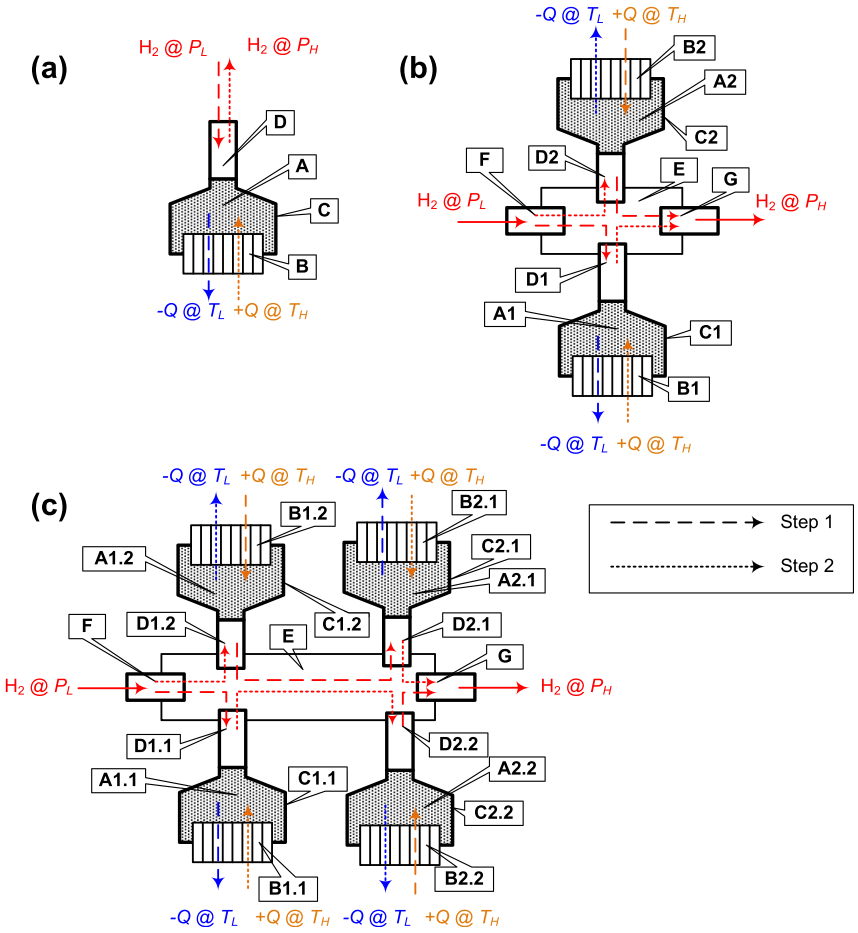

Fig. 7 – General layouts of MH compressor: (a) – periodically operated, (b) one-stage continuously-operated, (c) – two-stage continuously operated.

The assembly A–D called the metal hydride compression element, or generator-sorber, provides periodic suction of low-pressure hydrogen (H_2 @ P_L) when the MH is cooled (–Q) down to the lower temperature, T_L, followed by a discharge of high-pressure hydrogen (H_2 @ P_H) in the course of heating (+Q) of MH to the upper temperature, T_H. This solution first patented in 1970 by Wiswall and Reilly [66] allows periodically operated hydrogen compression that restricts its application from the continuous technological processes.

The simplest continuously-operated metal hydride hydrogen compressor (Fig. 7(b)) comprises two compression elements (A1–D1, A2–D2) similar to the one shown in Fig. 7(a). The gas pipelines D1 and D2 are connected to a gas distributing system (E) equipped with a port (F) for the supply of hydrogen at low pressure, P_L, and a port (G) for the output of hydrogen at high pressure, P_H. The operation of the compressor includes two steps, 1 and 2. During Step 1 the heat supply/removal accessory (B1) of the first compression element provides heat removal (–Q) from the MH (A1) at a lower temperature level, T_L; simultaneously, the accessory (B2) of the second compression element provides heat supply (+Q) to the MH (A2) at a higher temperature level, T_H. During the next Step 2 the heating/cooling modes of the accessories B1 and B2 are reversed, so that B1 operates in the heat supply, and B2 in heat removal mode. Thus, a periodic reversal of the operating modes of the heat supply/removal accessories B1 and B2 synchronised with switching gas flows by the gas distributing system (E) provides the continuous operation resulting in the suction of low-pressure hydrogen to the port F and the release of high-pressure hydrogen from the port G.

An approach to generate high H_2 pressures at modest operating temperatures is the use of multi-stage hydride compressors, a concept developed at Ergenics Inc. [98]. The multistage compressor uses a series of two or more alloys differing by thermal stabilities of their hydrides. Fig. 7(c) shows an example of layout of two-stage MH compressor. The alloy forming the most stable hydride is placed in the compression elements of the first stage (A1.1, A1.2), and other MH are loaded to the compression elements belonging to the next stages, in the order of decrease of their thermal stability (A2.1, A2.2). The multistage operation allows achievement of higher overall compression ratios using the same or smaller temperature swing. For example, five-stage MH compressor developed by Ergenics allows H_2 compression from 7 to 250 bar in the temperature range 30–90 °C with water as a heating/cooling agent [99].

The gas distributing system (E) can be made as a one-way (check) valve arrangement (see Fig. 8 as an example); the periodic heating/cooling of heat supply/removal accessories (B) is conveniently controlled by timing relays [100–102].

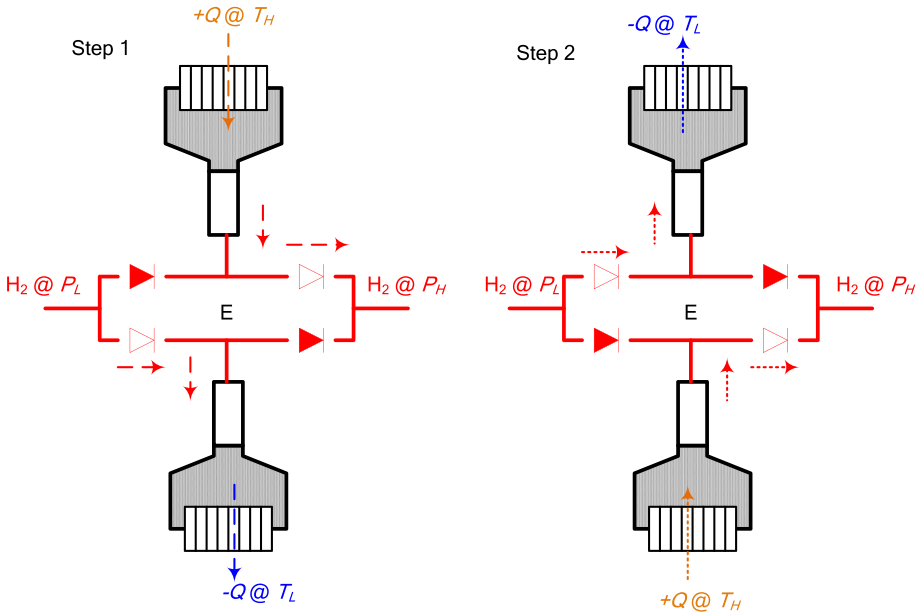

Fig. 8 – Operation of one-stage continuously operated MH compressor (Fig. 7(b)) when gas-distributing system (E) is made as a check valve arrangement. Opened and closed check valves are shown as empty and filled symbols, respectively.

The basic engineering approach described above is presented in a number of publications and patents. Before considering the details of its implementation (section 3.3), we would like to present thermodynamic analysis of the MH compressors as heat engines (next section), and to discuss efficiency of the compression.

3.2. *MH H_2 compressors as heat engines*

A detailed thermodynamic analysis of an MH hydrogen compressor (MHHC), or MH thermal sorption compressor (MH TSC), as a heat engine has been performed by Solovey [5,103,104]. Influence of various factors on thermodynamic performances of the MH TSC's was also considered in Refs. [57,89,105–110].

Hydrogen compression in an ideal MHHC/MH TSC (Fig. 9) is achieved by sequential processes which include:

(a) isobaric–isothermal absorption of low-pressure hydrogen ($P_1 = P_L$) at a lower temperature, T_L (1–2);
(b) polytropic heating of the MH from lower (T_L) to higher (T_H) temperature (2–3);
(c) isobaric–isothermal desorption of high-pressure hydrogen ($P_2 = P_H$) at higher temperature, T_H (3–4);
(d) polytropic cooling of the MH from T_H to T_L and isobaric cooling of high-pressure hydrogen from T_H to T_L (4–5–1).

When pressure–temperature dependence for H_2 absorption/desorption is described by the van't Hoff Equation (2), the heat, Q, will be transformed to compression work, W, with the efficiency of Carnot cycle (η_C) realised within the same temperature range:

$$W = Q\frac{T_H - T_L}{T_H}; \tag{8a}$$

$$\eta_C \equiv \frac{W}{Q} = \frac{T_H - T_L}{T_H}; \tag{8b}$$

where T_H and T_L are the temperatures of heat supply and heat sink, respectively.

Equation (8b) gives the upper limit of the MH TSC efficiency. The efficiency of the real engine will be reduced by two groups of factors described below.

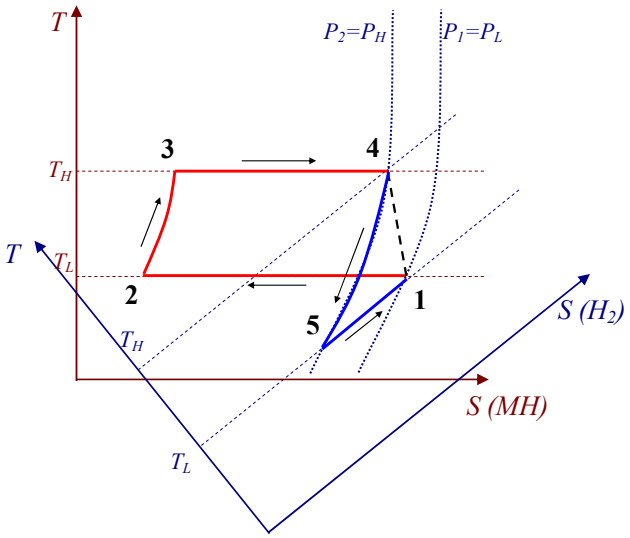

Fig. 9 – Entropy (for both metal hydride and hydrogen gas)–temperature diagram of the operation of an idealised MH compressor [104].

- The first group includes intrinsic factors characterising physical–chemical behaviour of the real system of hydrogen gas with hydride-forming materials. These are reversible hydrogen sorption capacity, plateau slope, hysteresis, and dilatation.
- The second group is related to the design and technological performance of the specific MH TSC's and their components (mainly, MH containers). These include rates of heat exchange between the heat transfer fluid and the MH bed, volume of the dead space (void fraction in the MH bed), material consumption of the MH container (containment/MH material weight ratio), and efficiency of heat recovery.

Reversible hydrogen storage capacity, ΔC, is a difference between hydrogen concentration in the MH at suction, $C_L(T_L, P_L')$, and discharge, $C_H(T_H, P_H')$, conditions (Fig. 3). It is determined by direct measurements of the pressure–composition isotherms for the MH alloy at T_L and T_H. If the detailed experimental PCT data for the MH are available, they can be fitted using a model for the PCT diagrams, and then the values of ΔC for different operating conditions can be easily evaluated (see Section 2.1). This factor influences the MH TSC efficiency both directly and, furthermore, via such engineering factors as dead space and material consumption. Increasing reversibility of the hydrogen storage capacity leads to the smaller differences between the MH TSC efficiency and its ideal (Carnot) value. These two values converge for a completely reversible H absorption–desorption.

The thermodynamic properties of the MH–hydrogen system are important both for adjusting hydrogen suction/discharge pressure to the available temperature range and for the achieving of the best possible efficiency of the MH TSC. First of all, this concerns the specific heat $Q \approx |\Delta H^0|$ of hydrogen sorption/desorption which determines thermal energy consumption during hydrogen compression. Specific heat capacity, c_p, of the MH alloy is also very important.

It should be noted that the correct calculations of the high-pressure MH TSC parameters should also take into account fugacity of hydrogen and temperature variation of the differences in heat capacities of the reagents participating in the Reaction (1). Neglecting these important features can introduce large errors when using the Van't Hoff Equation (2) values for the discharge pressures; these deviations can be up to 30% higher than the correct ones [89].

As briefly mentioned in the Section 2.1, in the plateau region the equilibrium pressure of hydrogen absorption exceeds the equilibrium pressure of hydrogen desorption. This factor, sorption hysteresis, is expressed quantitatively by a difference in free energy [13]:

$$\Delta G_{hyst} = RT \ln\left(\frac{P_A}{P_D}\right) \quad \text{or} \quad \delta_T = \ln\left(\frac{P_A}{P_D}\right) = \frac{\Delta G_{hyst}}{RT}; \tag{9}$$

where P_D and P_A are, respectively, desorption and adsorption hydrogen equilibrium pressures measured at the same temperature, and δ_T is isothermal hysteresis factor. This value is the characteristic of a specific MH–hydrogen system and should be determined experimentally. As it was shown in Ref. [103], hysteresis causes additional energy consumption required to close the thermodynamic cycle of an MH TSC. It causes losses in hydrogen compression work and, therefore, reduces the efficiency of hydrogen compression. In thermodynamic calculations of the MH TSC efficiency the hysteresis can be described by isobaric factor, δ_P which can be expressed as:

$$\delta_P = \frac{1}{T_A} - \frac{1}{T_D} \approx \frac{\Delta S_D^0 - \Delta S_A^0}{Q_S}; \tag{10}$$

where index A corresponds to absorption, index D for desorption and $Q_S \approx -\Delta H^0{}_A \approx -\Delta H^0{}_D$.

Another intrinsic factor indirectly influencing on the efficiency of the MH TSC is dilatation that is relative volume change resulting from expansion of the parent metal lattice in the course of the MH formation (see Section 2.3.4). The typical values of the dilatation coefficient, $\alpha = \Delta V/V_0$, are of 10–30% [6], see also Fig. 5. Dilatation causes changes in the MH density that influences on the value of the dead space in the MH TSC (see below) and, on the other hand, results in swelling of the MH bed that affects safety and reliability of MH containers.

The rate of heat transfer between the heat carrier and the MH bed is the most important design and technological factor affecting both the efficiency and productivity of the MH TSC. In efficiency calculations this factor is taken into account by taking T_H below the heating temperature and T_L above the cooling one; the differences are calculated starting from the effective overall heat transfer coefficients [105].

The disperse structure of the powdered MH bed, as well as presence of voids filled by gas in the MH container and gas distribution system determine the effect of the dead space, which negatively influences the MH TSC efficiency and productivity [45]. This negative influence increases with increasing discharge pressure. For example, at output pressure of 300 bar and typical value of a dead space of 0.25 cm^3 per 1 g of the MH alloy having hydrogen sorption capacity ~140 cm^3/g STP, the fall in both productivity and efficiency reaches 30% [89].

Influence of the dead space on the efficiency of MH TSC can be taken into account by introducing dimensionless coefficient K_V:

$$K_V = \frac{m_H(o) - m_H(i)}{m_H(MH)}; \tag{11}$$

where $m_H(o)$ and $m_H(i)$ are the weight (or number of moles) of H_2 in the dead space at output (discharge) and input (suction) conditions, respectively, and $m_H(MH)$ is the weight (or number of moles) of H_2 in the metal hydride (equal to the reversible hydrogen sorption capacity multiplied by the weight of the MH). K_V depends on conditions of hydrogen suction and discharge and, also, on the real and packing densities of the MH. Decreasing the dead space can be achieved first of all by increase of the MH bed packing density, taking into account safety requirements originated from swelling.

An important design factor affecting the MH TSC efficiency is material consumption of the MH container. It includes pressure containment and heat exchanger; these, being periodically heated/cooled, cause heat losses and decrease the MH TSC efficiency. The material consumption can be taken into account by introducing coefficient K_M equal to the ratio of the

total weight of the empty container to the weight of the MH therein. The negative influence of the material consumption can be partially mitigated by the heat recovery.

The quantification of the influence of the above-mentioned factors on the efficiency of the MH TSC, η, was derived by Solovey [5,103] as:

$$\eta = \frac{Q(\eta_C - \delta_P T_L)(1 - K_V)}{Q(1 - K_V) + (1 - \sigma)[c_\Sigma \frac{1+K_M}{\Delta C}(T_H - T_L) + QK_V]} \quad (12)$$

Here the numerator represents the net heat required for hydrogen compression, and denominator is the total supplied heat. Q is the net heat required for hydrogen desorption from the MH; η_C is the Carnot efficiency (Equation (8b)); δ_P is isobaric hysteresis factor (Equation (10)); K_V is the dead space coefficient (Equation (11)); σ is heat recovery efficiency; c_Σ is the total heat capacity of the MH container with MH bed; K_M is material consumption coefficient, and ΔC is reversible hydrogen sorption capacity expressed as hydrogen weight fraction in the MH.

Efficiencies of the MH TSC calculated using Equation (12) at various heat recovery efficiencies are shown in Fig. 10. The figure also contains our estimations of the efficiency range of industrial mechanical compressors produced by RIX Industries [111]. These compressors having the productivity of 50–100 m^3/h and compression ratio of 50–350 are characterised by the efficiency of 40–45%. This is superior to the efficiency of the MH compressors (below 25% at $T_H \sim 150$ °C). However, mechanical compressors also require significant investments from their operators and require much more directly generated electrical energy than the concept of the MH TSC that is based on utilisation of the waste thermal energy.

Calculations presented above assume that the energy inputs for the MH H_2 compression are associated only with the heating of the MH material from T_L to T_H, and the cooling from T_H to T_L is a spontaneous process of the heat dissipation into environment. If the cooling requires additional energy input

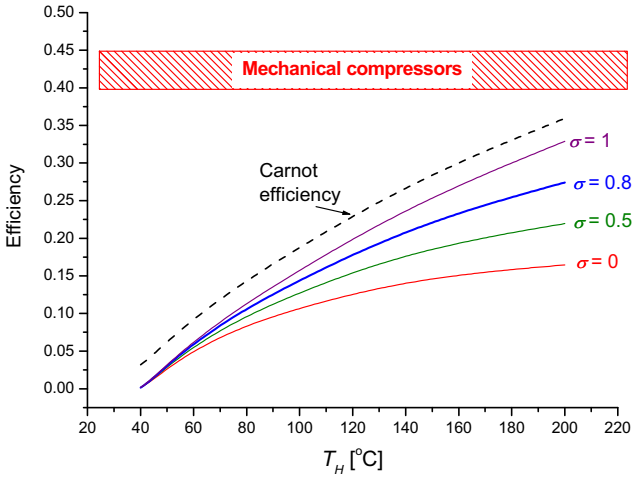

Fig. 10 – Efficiencies of MH TSC using $LaNi_5$ at $T_L = 30$ °C and different heat recovery efficiencies, σ: $\Delta C = 1.4$ wt.%; Q = 31 kJ/mol H_2, or 217 kJ/kg (MH); $\delta P = 2 \cdot 10^{-4}$ K^{-1}; $K_V = 0.1$; $K_M = 1.0$; $c_\Sigma = 0.51$ kJ/K.

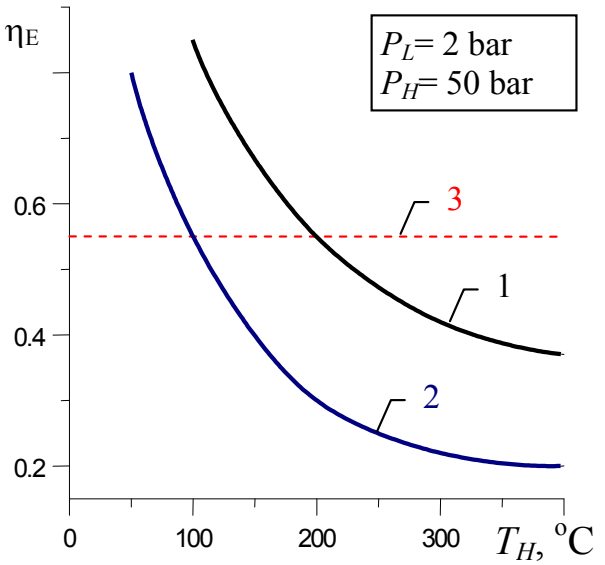

Fig. 11 – Exergy efficiency of single- (1) and two-stage (2) MH compressor and mechanical H_2 compressor (3) as function of heat source temperature [106].

(e.g., when a heat pump is used), the amount of consumed energy will be higher resulting in a decreased efficiency. Calculations by Kelly and Girdwood [110] for the H_2 compression from $P_L = 130$ bar ($T_L = 30$ °C) to $P_H = 414$ bar ($T_H = 130$ °C) yielded the efficiency of the process (related to the isothermal compression work) as 2.9%, or 11.6% of the Carnot efficiency. According to our calculations using Equation (12) (no heat recovery) and parameters presented in Ref. [110], the corresponding values are 7 and 28%, respectively. The origin of the difference is in the accounting of the energy input used for the cooling (about 51% of the total energy consumption) applied in Ref. [110].

Low energy efficiency is a common feature of heat engines operating in a narrow temperature window (Equation (8)). Various energy losses in the real MH compressors result in further decrease of their efficiency. Finally, as it was shown in the previous paragraph, the efficiency further decreases because of additional energy inputs. Therefore, the MH hydrogen compression can become beneficial either for some special applications, or when the energy inputs are associated only with low-grade waste heat.

Analysis of the value/exergy of primary energy inputs consumed in the thermally driven MH H_2 compression can be a useful tool in the comparison of this method with conventional compression technologies.

Fig. 11 shows calculated exergy efficiencies of the MH and mechanical electrically driven hydrogen compressors [106]. There the single-stage MH TSC based on $LaNi_5$ intermetallic compound, and two-stage MH TSC using $LaNi_5$ for the first stage and $Ce_{0.5}La_{0.5}Ni_5$ for the second one were considered. The total heat capacity of the containment was assumed to be equal to the heat capacity of the MH ($K_M = 1$), and the efficiency of heat recovery (σ) was assumed to be 0.5. It can be seen from Fig. 11 that MH hydrogen compression can provide the efficiency gain over mechanical one at the temperatures below 200 °C for a single-stage MH TSC and below 100 °C for a

two-stage MH TSC. For these conditions a significant energy benefit in comparison with mechanical compression takes place. It also can be seen that an increase in the number of stages of an MH compressor results in a significant decrease of its efficiency. Thus, the number of compression stages for large-scale industrial applications should be minimised.

The contribution of factors influencing the exergy efficiency of the MH compressors is shown in Fig. 12 [104]. The efficiency of heat transformation into the energy of the compressed H_2 was found to be about 0.58 that corresponds well to the data for one stage MH compressor at $T_H \sim 100$ °C (Fig. 11). It was also noted in Ref. [104] that if to consider exergy efficiency of electrically-driven mechanical compressors starting from the heating value of a fuel burnt at a thermal power plant (efficiency about 0.4) then the efficiency will be about 0.18, or 3.2 times lower.

As can be seen from Fig. 12, the major factors contributing to the decrease of the efficiency of MH compressors are transient losses (1) and losses caused by heat transfer (2). Reduction of these losses is the main objective of further improvements in design and operation features of the MH hydrogen compressors which will be considered in the next section.

3.3. *Design features and performances*

Improvement of the basic engineering approach in the development of MH hydrogen compressors (section 3.1) mainly concerns:

(i) Optimisation of the hydride-forming alloys;
(ii) Design of compression elements;
(iii) Methods and accessories for heat supply/removal;
(iv) Number of compression elements, their gas connections and the sequence of operation of the associated heat supply/removal accessories.

The approach to the selection/engineering of the MH materials, mainly related to the adjustment of the required operating pressures over the available temperature range, was considered in section 2. The present section will consider the engineering solutions of MH containers to be critical components of the MH compressors (section 3.3.1) and system features followed by a brief overview of state of the art in the international development of MH compressors (3.3.2).

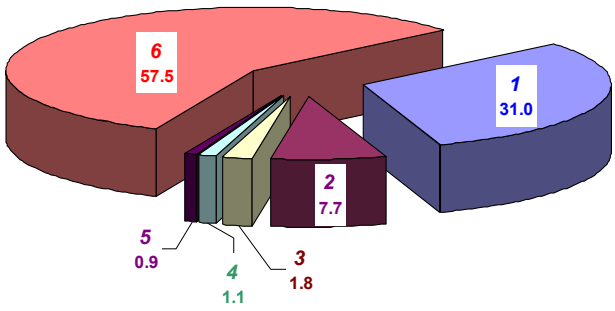

Fig. 12 – Exergy balance (in % to the exergy of heat at T_H) for H_2 compression using MH [104]: 1 – losses in transient process; 2 – losses caused by heat transfer; 3 – losses for dead space; 4 – losses due to heat transfer with the environment; 5 – losses in gas distribution system; 6 – useful exergy.

3.3.1. *MH containers/compression elements*

A proper design of the containment for the MH material for H_2 compression, together with the associated H_2 gas and heat supply/removal accessories, has two main objectives. First of all, it aims at the achievement of high hydrogen charge–discharge rates to provide shorter cycle time and higher productivity of the compressor. Secondly, it has to provide higher efficiency of hydrogen compressors by reducing the losses (see Fig. 12).

The main problem to be solved for the achievement of both goals is the intensification of heat transfer between the heat supply/removal accessories and the MH material. The main factor limiting the H_2 charge/discharge dynamics of the MH containers is the low thermal conductivity of the powdered hydride beds [45]. Moreover, its value is strongly related to both design and technological parameters (geometry, MH packing density, as well as the wall heat transfer resistance), and on the operation conditions. Usually, the effective thermal conductivity of a powdered MH bed can vary in the range of 0.13–2.3 W/(m K) while the thermal conductivity of a bulk alloy is more than order of magnitude higher, e.g. 30 W/(m K) for $LaNi_5$ [7].

Optimisation of the MH bed heat transfer performances requires their modelling and verification by comparison with experimental data. The MH bed heat transfer modelling (with a subtask of hydrogen mass transfer) was developed rather intensively during the last three decades. Various computation and experimental approaches are presented, for example, in Refs. [47,50,90,112–126].

A conventional way to improve the heat transfer characteristics of the MH bed is in increase of the surface area of heat exchange and reduction of the characteristic heat exchange distances. It can be done, for example, by using long tubular MH containers of a small diameter used in the compressor where simultaneously heated/cooled containers are immersed into one heating/cooling jacket [101]. The "shell-and-tube" solution can be used for both separation/purification and compression of hydrogen [127]. Application of tubular containers, 12–25 mm in outer diameter filled with 150–900 g of MH powder allows to achieve a reasonable duration of H_2 absorption/desorption (half-cycle time), 5–10 min [58,75,128]. The necessary hydrogen storage capacity can be achieved by connecting several containers in parallel; as example, compression element of industrial scale MH compressor (up to 14 kg of MH) comprises of sixteen tubular MH containers immersed into a common heating/cooling jacket [58]. Additional intensification of the heat exchange between the heating/cooling fluid and the external surface of the MH containers is achieved by use of fins [75], or thermally conductive metal blocks [128].

Effect of the aspect ratio of the tubular MH containers on their performances was studied in Ref. [124]. The issues of modelling and optimisation of multi-tubular MH beds were considered in Ref. [117]. A typical engineering solution of hydrogen storage and supply device composed of tubes filled with MH is presented in a patent [131].

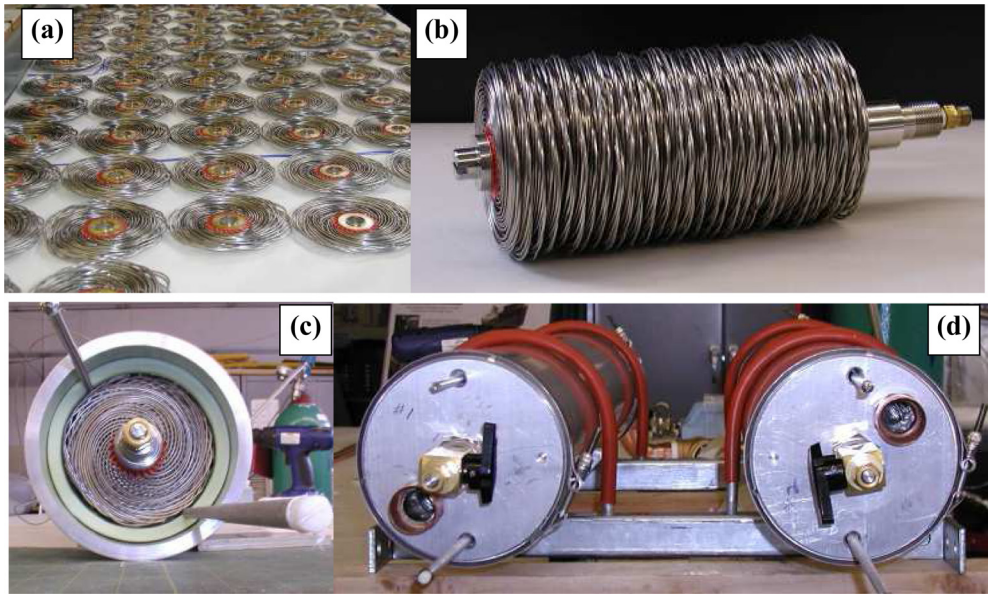

Fig. 13 – 1/16″ OD hydride tube ring manifolds (a), the manifolds stacked into hydride heat exchanger (b), the placement of the heat exchanger in MH compression element (c), and two-element 3-stage MH compressor assembly (d). Adopted from Linde–MRT–Ergenics joint presentation [135].

Apart from a decrease of characteristic heat transfer distance, the decrease of the diameter of the tubular MH container allows to reduce the material consumption because a pressure vessel with a smaller diameter can have a thinner wall for the same pressure rating. This results in a significant increase of the efficiency, due to reduction of transient losses for periodic heating/cooling of the containment (see section 3.2).

The best realisation of the approach described above was achieved by Ergenics [129,130,132–136]. Metal hydride material is loaded into a tubular containment having a small outer diameter, down to 1/16″, or 1.588 mm. The intensification of heat exchange between the outer surface of the hydride tube and heating/cooling fluid can be achieved by fins formed by steel wire wound and soldered onto the hydride tube [132–134]. It allows hydride beds to be thermally cycled at a rapid rate (<1 min) resulting in high productivities. The outer "spring" formed by the wound wire also reinforces the hydride/hydrogen containment allowing for its safe operation at high pressures. Alternative solutions [129,130] include placement of the "spring" inside the cylindrical containment, so the MH becomes located in between the inner surface of the cylinder and the outer surface of the spring; thus allowing compensation of the MH swelling effects during the hydrogenation.

A plurality of the hydride tubes can be assembled in an MH reactor combining features of the hydrogen manifold and heat exchanger (Fig. 13). The designs of the reactors are modular, resulting in a high volume low cost production.

Intensification of heat transfer in the larger MH containers can be achieved by a placement of the MH material within a heat transfer matrix inside the containment. The MH containers have built-in heating and cooling accessories thermally coupled with the heat transfer matrix, as well as the pipelines for supplying hydrogen gas to and receiving hydrogen gas from the MH. These elements are present in numerous developments of the MH containers.

A typical approach is shown in Fig. 14. It is used for the medium-scale MH-based hydrogen storage and compression. The MH container is made as a cylindrical gas-proof containment equipped with end caps. The MH material is placed inside the containment (1) into a heat transfer matrix to form a metal hydride bed (2). Hydrogen input/output (3) is provided by an axial pipe (3.1) installed at one end cap and usually ended by an inline gas filter (3.2). Heating and cooling is provided by a heat transfer fluid (e.g., water) running through either external heating/cooling jacket (A) or core tube of the inner heat exchanger (B) (4).

The main solutions utilising such an approach include:

- Type of the heating/cooling:
  - flow of heat transfer fluid for both heating and cooling [97–100,108–110,137,138]; this solution is used in most cases [58,75,101,129–134];
  - electric heating, in combination with convective (natural or forced) air cooling [66,139–141];
  - electric heating, liquid cooling [71,102,128,139,140];
  - electric heating, cooling using a cold radiator thermally coupled with MH bed through a gas-gap thermal switch [142,143];
  - heat-pumping systems including thermoelectric (Peltier) modules [96,144];
  - heat pipes, in combination with electric heaters or catalytic combustors (heating) and flow of liquid or gaseous heat transfer fluid (cooling) [145,146].
- Placement of the heating/cooling means with respect to the containment:
  - external [58,75,96,109,117,118,137,140];

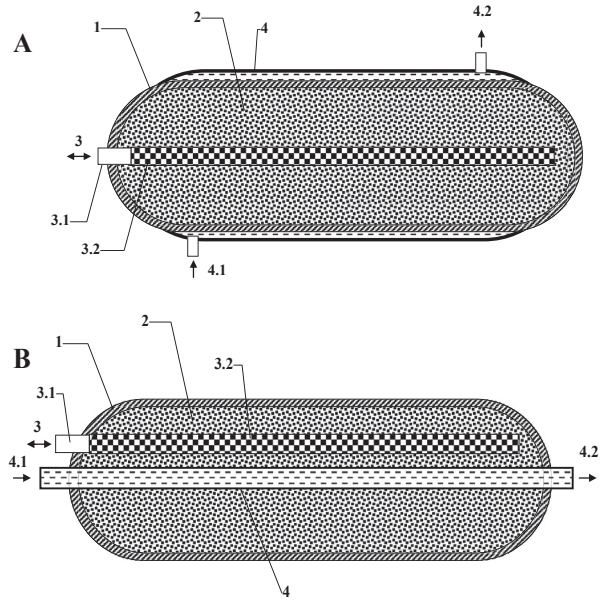

Fig. 14 – Typical layouts of the MH containers with external (A) and internal (B) heating/cooling by a flow of heat transfer fluid: 1 – gas-proof containment; 2 – metal hydride bed (MH material + heat transfer matrix); 3 – H_2 in/out line: 3.1 – H_2 inlet/outlet pipeline, 3.2 – gas filter; 4 – heating/cooling jacket (A) or core tube of inner heat exchanger (B): 4.1 – input and 4.2 – output of heat transfer fluid.

- internal [94–97,125,126,145,146];
- combined [102,128,140–142].

- Type and layout of the heat transfer matrix, including:
  - heat-conductive fins [10,94,97,125,126,137,145–152];
  - coiled tube heat exchanger [126,147,153];
  - metal foams [10,124,138,142,154,155] or honeycomb metallic structures [122]; an alternative arrangement of the metal foams with the fins was shown to be very efficient [10];
  - a simple and efficient method of the forming of the MH bed is in the compacting of the powders of an MH and a heat-conductive material, including porous metals [109,156–158] or expanded natural graphite, ENG [159–162]. An alternative arrangement of the MH/ENG compacts with the fins was patented in Ref. [163]. Significant improvement in effective thermal conductivity in MH–carbon composites was recently observed in a course of direct deposition of single-wall carbon nanotubes on the surface of particles of the hydride-forming alloy [164]. The details on the preparation of the MH/ENG compacts on the basis of AB_2-type alloys suitable for high-pressure applications were recently reported in Ref. [165].

It has to be noted that performances of the metal hydride compressors and its main element, metal hydride container, are strongly dependent on numerous factors that include the following conflicting trends [97,137]:

- The reduction in the size (diameter) of the container, results in better hydrogen absorption/desorption dynamic performances, and, in turn, in the shortening the operation cycle time. Correspondingly, the specific productivity per unit of weight of the MH material is increased. At the same time, due to kinetic limitations (see section 2.2), this improvement has a maximum limit, and it seems unfeasible to achieve the half-cycle time shorter than 1–2 min. Thus, high total output productivity for smaller containers can be achieved by the increase of their number in a compression element. However, large increase in the number of the hydride containers will result in the increase of the number of joints in the corresponding gas manifolds and will also increase the probability of leaks that has a drawback from the safety and reliability viewpoints.
- Although shortening of the cycle time increases the productivity of the MH compressor, it has a negative influence on the operation lifetime, due to the degradation of the MH (section 2.3.3). The service life of an MH material at specified pressure/temperature conditions is determined by a number of hydrogen absorption/desorption cycles ($\sim 10^4$ when operated in pure hydrogen at $T < 200$ °C and $P_{H_2} < 200$ bar), and for the shorter times of the operation cycle the lifetime of the compressor will be decreased.
- The required total output productivity can be also increased by the increase of the amount of MH material in the compression element, particularly, by the increase of the size of the MH container. However, the drawback is a longer operation cycle. Introduction of special heat distribution means/heat transfer matrix results in an increase of the material consumption and, in turn, the total heat capacity of the MH container. The same effect has the increase in the diameter of MH container itself, since to withstand the operating pressure the containment should have thicker walls that results in the increase of the total heat capacity. It significantly increases transient losses and reduces the efficiency (section 3.2). Reducing the weight of the high-pressure containment can be achieved by the application of a "hybrid" solution where MH material is distributed inside a composite cylinder having a lightweight multilayer structure. Usually, this solution is used for weight-efficient hydrogen storage [166,167], but modifications that can be adopted for MH hydrogen compression are also known [137,145,146]. Mainly the adaptations are related to the reduction of the dead space in the inner volume of the MH container.
- Decrease of the dead space is very critical for increasing efficiency of high-pressure hydrogen compression applications [89]. First of all, it is achieved by the increase of the filling fraction for the MH material. However, due to the "swelling" effects, there exists an upper limit (61% of the density of the hydrogenated material) of the filling density to provide safe operation (see section 2.3.4). The secondary effect is in further pulverisation of MH in the course of hydrogen absorption/desorption cycling that causes concentration and agglomeration of MH particles in the lower parts of the containment [168]. The common way to mitigate this effect is to keep rather large length/diameter ratio and to place the container horizontally.

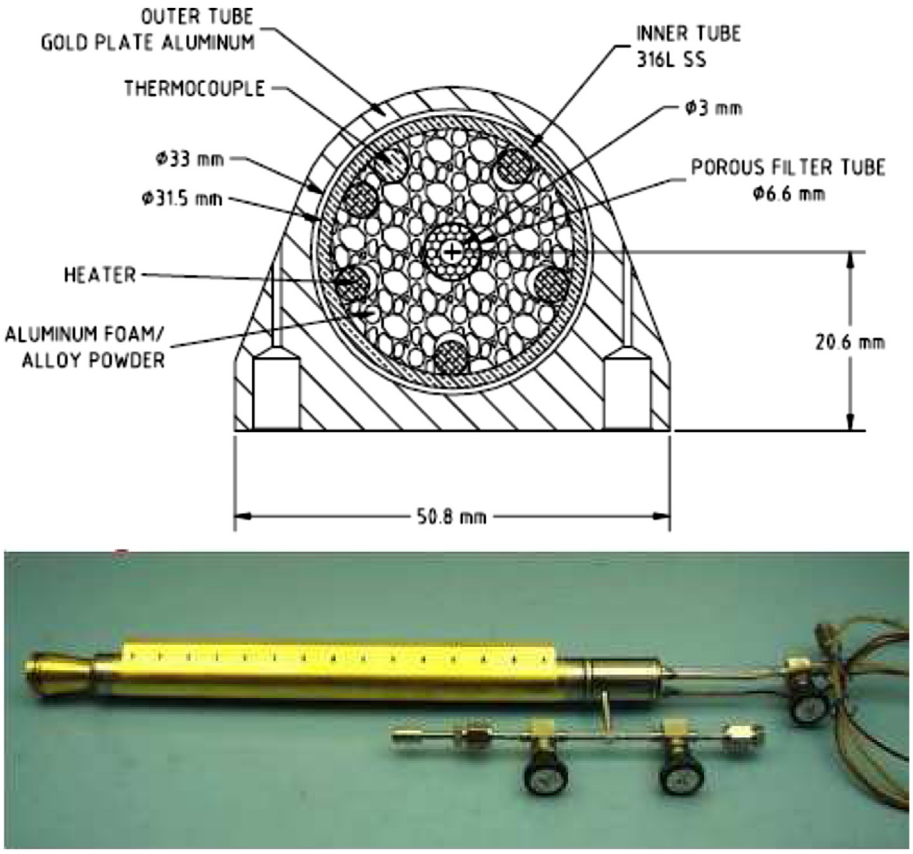

Fig. 15 – Cross section (top) and general view of MH container/compression element for space applications [142].

In summary, we can conclude that any particular realisation of MH containers/compression elements strongly depends on the specific application requirements.

For the smaller-size applications, operation performances (first of all, productivity) are most important, and the corresponding solutions envisage forced heating and cooling of thin (≤10 mm) MH beds incorporating MH material and heat distribution means (metal foams/fins). Fig. 15 presents an example of the MH container developed by Jet Propulsion Laboratory/NASA as a compression element for 0.6–50 bar, 260 L H_2/h hydrogen compressor for hydrogen sorption cryocooler used in on-board hydrogen Joule–Thomson cryocoolers for the ESA Planck mission [142]. The compression element provides fast desorption of the high pressure H_2 due to electric heating of the MH bed (615 g of $LaNi_{4.78}Sn_{0.22}$ dispersed in aluminium foam). The cooling is provided by a cold (<0 °C) radiator thermally coupled with the outside of the container via 0.75 mm thick gas gap heat switch. The latter couples or isolates the bed with the radiator, by the variation of the pressure of H_2 gas ($\sim 10^3$–10^{-2} Pa) using periodic H_2 desorption–absorption by ZrNi intermetallic alloy. Further intensification of the MH cooling can be achieved by, for example, use of thermoelectric coolers/Peltier modules [96].

For the medium- and large-scale applications efficiency and manufacturing cost become crucial. It poses a motivation for the usage of the available waste heat sources such as steam and hot water. The corresponding solutions, as a rule, include quite large MH containers (≥10 kg MH) heated/cooled by a flow of heat transfer fluid (hot/cold water or oil, steam/water, etc.). Typically, heat distribution is provided by heat conductive fins disposed within the MH powder [94,97,137,145,146, etc.]. Fig. 16 presents an example of the MH container for H_2 compressor (up to 200 bar) that comprises of 12–15 kg of MH powder (1500 to 2000 L H_2 STP storage capacity) and uses wet steam (up to 140 °C) or super-heated water (up to 180 °C) for the heating [94,97] providing up to 200 bar H_2 output pressure and hour productivity up to 1000 L H_2 STP. The container showed satisfactory hydrogen compression performances when typical half-cycle duration (H_2 absorption or desorption) was about 30 min [97]. Further increase of the size of MH container for H_2 compression (about 1 m long, 200 mm internal diameter, MH load 45 kg) was shown to result in significantly longer (>1 h) H_2 desorption time because of the less efficient H_2 mass transfer inside the container [169].

3.3.2. *Integrated compression systems*

Table 2 presents summary of design features and performances of the MH compressors developed since the publication of the first patent [66] describing application of MH for H_2 compression.

Main design features of the MH compressors include type(s) of the used hydride-forming material(s), mode of operation (periodic or continuous), as well as number of compression stages.

Integration of MH containers for H_2 compression (Section 3.3.1) into compressor assemblies realises one of the general layouts schematically shown in Fig. 7. The corresponding

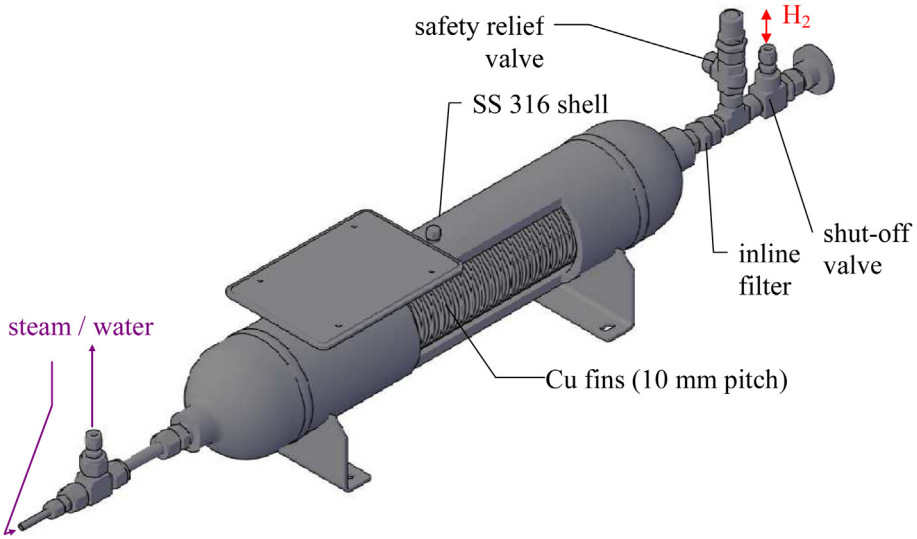

Fig. 16 – Metal hydride container for medium-to-large scale H_2 compression applications.

engineering solutions are mainly related to (i) selection of number of stages and proper MH material(s) allowing to achieve the required H_2 compression in the available heating/cooling temperature range; (ii) design of the gas-distributing system; (iii) management of periodic heating and cooling of the MH containers; (iv) control and automation of operation; and (v) solutions aimed at the increase of compressor's efficiency.

As a first step of the selection of MH material, the thermodynamic approach described in Section 2.1 can be used. It should be noted that the selection has to foresee a certain margin in the material's performances, i.e. for the compression stage operating between T_L and T_H, the value of P_L should be lower and the value of P_H higher than H_2 suction and discharge pressures, respectively. This will provide a driving force necessary to achieve acceptable rates of the H absorption and desorption processes. Further evaluation of charge/discharge dynamic performances of the selected design of MH container (see previous section) will allow one to determine required number of the containers in an assembly, and to estimate important performance characteristics, like cycle productivity, cycle time, consumption of power or heating/cooling fluids, etc.

One-stage periodically operated MH compressors usually comprise one (Fig. 7(a)) or several connected in parallel MH containers/compression elements. They normally have a simple gas-distributing system on the basis of shut-off valves which provides connection of a gas manifold of a cooled compression element to low-pressure H_2 input and, when the compression element is heated up, to high-pressure H_2 output port of the compressor. Due to its simplicity and flexibility, this solution found numerous applications (see Table 2), mainly in laboratory practice. In combination with electric heating to moderately high temperatures (~500 °C), it can provide generation of very high hydrogen pressures, up to 5 kbar [179]; another option to generate kilobar-range H_2 pressures is in a combination of MH compression (first stage, up to 400 bar) with the cryogenic cooling–heating cycle (second stage) [176].

In a multistage periodically-operated MH compressors gas manifolds of the stages are connected sequentially in the ascending order; opening and closing of the valves is synchronised with the alternate periodic heating and cooling of the compression elements, e.g. stages 1, 3 ↔ stage 2 for the three-stage compressor (see example in Ref. [138]).

The gas-distributing systems of continuously-operating MH compressors provide switching of H_2 flow passing from a low-pressure input port to gas manifold of the cooled compression element(s) of the first stage, further from gas manifolds of the heated compression elements to the cooled compression elements of the next stage, and, finally, from gas manifold of the heated compression elements of the last stage to the high-pressure H_2 output port (see Fig. 7(b, c)). The switching can be provided by manual or remotely actuated shut-off valves whose operation must be synchronised with periodic heating and cooling of the compression elements. A commonly-used solution which allows to simplify the compressor assembly and to reduce its cost is in the usage of one-way (check) valves (Fig. 8) which automatically provide flowing of H_2 from higher pressure manifolds to lower pressure ones, so that the operation of the compressor can be achieved only by thermal management (see, e.g. Refs. [100–102]). The check valve solution is similar to the one conventionally applied in mechanical compressors. However, the heat-driven MH compressors significantly differ from their mechanical analogs by much slower rate of pressure increase/decrease when passing from charge to discharge mode and vice versa. Typical duration of the charge/discharge cycle in MH hydrogen compressors varies from ~1 to ≥30 min that is much longer than the duration of the conventional mechanical compression cycle (≪1 s). This fact increases the probability of malfunction of the check valves resulting in an H_2 backflow. Thus, when introducing check valves in gas-distributing system of MH compressor assembly, special attention has to be paid to the measures decreasing a probability of the backflow. According to the authors' experience, the problem can be addressed by a proper selection of the check valves (non-rotating stem and high enough cracking

Table 2 – MH H_2 compressors developed in 1970–2013.

Year	Design features				Performances							Developer; notes	Ref.
	Operation	# of stages	# of containers per stage	Hydride-forming material	T_L [°C]	P_L [bar]	T_H [°C]	P_H [bar]	Productivity [m^3/h STP]	Half-cycle duration [min]	Efficiency [%]		
1	2	3	4	5	6	7	8	9	10	11	12	13	14
1970	Periodic	1	1	TiFe (60 g)	20	35	137 (200)	255 (690)	No data			*US Atomic Energy Commission*; electric heating, convective cooling	[66]
1971	Periodic	1	1	VH_x (100 g)	18	7	50	24	0.072	1	No data	*Brookhaven NL (US)*; water heating/cooling[a]	[62]
1979	Continuous	1	2	$LaNi_5$ (700 g)	20	2.5	80	20	No data	2	7.7	*National Chemical Laboratory for Industry (JP)*; water heating/cooling, 28 W mechanical power output	[170]
1980	Periodic	1	1	$LaNi_{4.63}Al_{0.37}$ (1.5 kg)	23	1.2	68	2.1–3.3	No data	3–16	1.6–2.4	*Sandia NL (US)*; water heating/cooling, water pump:/15 L per cycle	[171]
1983	Periodic	1	19	$LaNi_5$ (19 × 0.91 kg)	27	3	90[b]	18	21.6	3	14.2[c]	*Tsukuba Research Centre (JP)*; used for desalination by reverse osmosis, water heating/cooling (30 L/min)	[148]
1990s	Continuous	4–6	No data	AB_5	25	1–4	85	40–200	Up to 2.5	2	No data	*Ergenics Inc (US)*; commercial series, 20 years life time	[172]
1993	Continuous	1	3	TiFe + 2 wt.% Mm (3 × 1 kg)	20	10	250	100	0.42	15	4–7	*Universidade Estadual de Campinas (BR)*; water cooling–water/electric heating	[71]
1995	Periodic	1	3	$LaNi_5$ (3 × 1.5 kg)	25	10	370	150	1.4	45	3.9[c]	*Inst. Probl. Mech. Eng. (UA)*; electric heating (3 kW in total), convective cooling; 106 dm^3 volume; 46 kg weight	[139]
1995	Periodic	1	7	$LaNi_5$ (7 × 1.4 kg)	25	10	370	300	0.7	120	0.92[c]	*Inst. Probl. Mech. Eng. (UA)*; electric heating (8 kW in total), convective cooling; 170 dm^3 volume; 142 kg weight	[139]
1996	Periodic	3	1	1 – ZrNi (0.225 kg) 2 – $LaNi_{4.8}Sn_{0.2}$ (0.92 kg) 3 – $LaNi_{4.8}Sn_{0.2}$ (1.5 kg)	25	0.001	1–280 2–95 3–240	1–1 2–3 3–103	N/A			*NASA-JPL. (US)*; Electric heating (245 W), radiator cooling; hydride beds mass 57 kg, Space Shuttle flight.	[173–175]
1998	Continuous	2	30	1 – $LaNi_{4.5}Mn_{0.5}$ (30 × 1.33 kg) 2 – $LaNi_5$ (30 × 1.33 kg)	25	3	250	150	10	35	4.48[c]	*Inst. Probl. Mech. Eng. (UA)*; electric heating, forced air cooling (27 kW in total); size 2350 × 1150 × 1050 mm; 700 kg weight	[141]
1999	Periodic	1	1	$MmNi_5$ (1.6 kg);	15	25	327	400[d]	0.24	60	2.44[c]	*Inst. Probl. Mech. Eng. (UA)*; electric heating (1 kW), air cooling	[176]

(*continued on next page*)

Table 2 – (*continued*)

Year	Design features				Performances							Developer; notes	Ref.
	Operation	# of stages	# of containers per stage	Hydride-forming material	T_L [°C]	P_L [bar]	T_H [°C]	P_H [bar]	Productivity [m^3/h STP]	Half-cycle duration [min]	Efficiency [%]		
1	2	3	4	5	6	7	8	9	10	11	12	13	14
1999	Periodic	2 3	1 1	1 – Hydralloy C2 (AB_2) 2 – Hydralloy C0 ($TiMn_{1.5}V_{0.45}Fe_{0.1}$) 3 – $TiCrMn_{0.55}Fe_{0.30}V_{0.15}$ 1 kg each	20 20	12–18 30	60 60	85–110 200	No data	40–60	No data	*Helsinki Univ. of Technology (FI)*; water heating/cooling; combined compressor and heat pump, medium temperature ~30 °C heat upgrade/thermal efficiency 1.3–1.5.	[177]
2000s	Continuous	No data			25	0.8	100	300	1	No data		*Industrial Technology Research Inst. (TW)*; Commercial series	[178]
2001	Periodic	1	1	VH_x	20	100	527	5000	No data			*Russian Federal Nuclear Center*; air cooling/electric heating; research facility for H_2 and D_2 compression	[179]
2001	Continuous	1	No data	AB_5	25	20	400	345	0.33	16	No data	*Ergenics Inc (US)*; air cooling/electric heating; prototype; dimensions of heat exchanger in MH bed D250 × 500 mm	[133]
2002	Continuous	1	6	$LaNi_{4.78}Sn_{0.22}$ (6 × 615 g)	−7	0.6	197	50	0.26	60	8.68[c]	*NASA–JPL (US)*; chiller plate cooling/electric heating (410 W); used for the cryo-cooling on-board of Planck spacecraft; MH bed ~500 × 51 × 51 mm; lifetime ~20,000 cycles	[142]
2004	Continuous	No data				1	No data	350	No data		15	*Ergenics Inc (US)*; heating by natural gas	[134]
2005	Periodic	1	1	$MmNi_{4.6}Al_{0.4}$ (0.4 kg)	20	5	95	43.8	0.34	4.2	7.3	*Indian Inst. of Technology*; liquid heating/cooling (1–3 L/min)	[151]
2006	Periodic	3	1	1 – $LaNi_{4.8}Sn_{0.2}$, 2 – $LmNi_{4.9}Sn_{0.1}$, 3 – $MmNi_{4.7}Al_{0.3}$ (25 g each)	20	1	80	20	0.02	8–20	5	*Institut de Recherche sur l'Hydrogène (CA)*; water heating/cooling; pre-compression of H_2 from alcaline electrolyser	[138,180]
2007	Periodic	1	1	$Mm_{0.7}Ca_{0.2}La_{0.1}(Ni_{4.95}Al_{0.05})$, 1000 L H_2 capacity	25	40	170	450	2.4	15	No data	*Zhejang University (CN)*; oil heating/cooling	[181]
		2	1	1 – $Mm_{0.2}La_{0.6}Ca_{0.2}Ni_5$ 2 – $Ti_{1.1}Cr_{1.5}Mn_{0.4}V_{0.1}$	25	40	99	450	1.2	15		*Zhejang University (CN)*; water heating/cooling	
2008	Continuous	3	No data		20 (?)	0.5	90 (?)	100/435[e]	15	50 s	69[f]	*Ergenics Inc (US)*; liquid heating/cooling; module productivity >215 L/m[g]	[135,136]
2009	Continuous	2	4	1 – $(La,Ce)Ni_5$ (160 g); 2 – $(Ti,Zr)(Fe,Mn,Cr,Ni)_2$ (120 g)	15	7	110	200	0.06	10	1.6	*Univ. Western Cape (ZA)*; electric heating (400 W), water cooling	[128]

2009	Periodic	2	1	1 − $LaNi_{4.25}Al_{0.75}$ (3.5 kg) 2 − $LaNi_{4.8}Sn_{0.2}$ (45 kg)	50	16…0.2	175	33	1.02	30(ABS) 190(DES)	2.3	*Tech. Univ. of Lodz (PL)*; oil heating/cooling; 1/13 model of compressor necessary for operation of H_2 hardening furnace	[182]
2009	Periodic	3	1	1 − $LaNi_{4.85}Al_{0.15}$, 2 − $LaNi_{4.9}Cu_{0.1}$, 3 − $MmNi_{4.05}Fe_{0.95}$; 120 g each	20	2	80	56	0.3	2	No data	*Nat. Inst. for R&D of Isotopic and Molecular Technologies (RO)*; water heating/cooling	[183]
2010	Periodic	2	1	1 − $La_{0.35}Ce_{0.45}Ca_{0.2}Ni_{4.95}Al_{0}$05 2 − $Ti_{0.8}Zr_{0.2}Cr_{0.95}Fe_{0.95}V_{0.}$1 27 kg in total	25	50	150	700	2	60	No data	*Zhejang University (CN)*; oil heating/cooling[h]	[184]
2011	Periodic	1	3	$LaNi_5$, $Ca_{0.6}Mm_{0.4}Ni_5$, $Ca_{0.2}Mm_{0.8}Ni_5$.	10	13−40	90	100−150	No data			*Joint US−KR team*; water heating/cooling; MH: compacts of Cu-encapsulated IMC particles (5/3 g) with Sn binder (0.5/0.3 g), 170−200 bar compacting pressure.	[158]
		2	3	1 − $LaNi_5$; 2 − $LaNi_5$, $Ca_{0.6}Mm_{0.4}Ni_5$, $Ca_{0.2}Mm_{0.8}Ni_5$.	10	7	125	100−160					
2012	Continuous	2	6	1 − $LaNi_5$ (6 × 14 kg); 2 − $La_{0.5}Ce_{0.5}Ni_5$ (6 × 10 kg)	10−15	2−5	150	150−160	15	10	No data	*Russian Acad. Sci; Spec. Design & Engineering Bureau in Electrochemistry (RU)*; water cooling, steam heating.	[58]
2012	Continuous	2	2	1 − (La,Ce)Ni_5 (2 × 15 kg); 2 − $(Ti,Zr)(Fe,Mn,Cr,Ni)_2$ (2 × 12 kg)	20	10	120	200	1	30	1.65	*Univ. Western Cape (ZA)*; water cooling, steam or overheated water heating.	[94]
2012	Periodic	1	1	1 − $La_{0.4}Y_{0.6}Ni_{4.8}Al_{0.2}$ (594 g)	20	20	175	350	0.19	6	No data	*Inst. of Refrigeration and Cryogenics Eng., Shanghai Jiaotong Univ. (CN)*; water cooling, water/oil[i] heating.	[75]
		2	1	2 − V/$LaNi_5$ (594 g)	20/80[i]	20	95/175[i]	380	0.28				
2012	Continuous	2	1	1 − AB_5; 2 − AB_2	50	160	190	600	No data	40	No data	*Univ. of Birmingham (UK)*; oil heating, water cooling	[185,186]
2013	Continuous	2	3	1 − AB_5; 2 − AB_2	30	10−30	120	200	5−10	No data		*HYSTORSYS AS (NO)*; oil heating/cooling	[187,188]

[a] Adopted for pumping hydrogen and tritium mixture by pressure transmission via mercury U-tube.
[b] 86 °C at the output, the value of ΔT_H was used for the estimation of the consumed heat for efficiency calculations.
[c] The efficiency has been calculated by the authors of this review starting from the performance data.
[d] Up to 4000 bar using the second, cryogenic stage.
[e] Planned.
[f] As presented in the original works, most probably, this is % of Carnot efficiency (19.3% for the specified temperature range).
[g] Miniature hydride heat exchangers retain hydride alloy within 1/16″ OD Tubes.
[h] Stage 1 − capacity 2000 L, Stage 2 − capacity 1000 L. 300−400 bar at 1st stage (separate collection to the receiver).
[i] For stages 1/2.

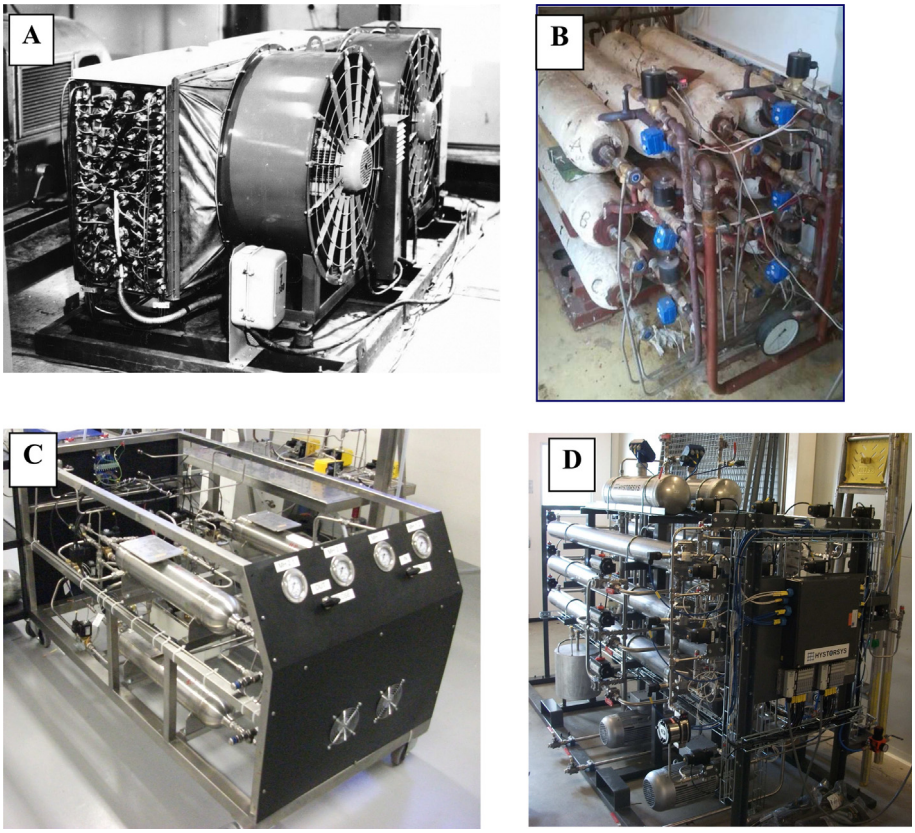

Fig. 17 – Medium-to-large scale MH compressors: A – Institute for Mechanical Engineering Problems of the National Academy of Sciences of Ukraine (1998, 3–150 bar/10 m^3/h) [141]; B – Institute of Problems of Chemical Physics/Russian Academy of Science, Special Design Engineering Bureau in Electrochemistry, Russia (2012, 2–160 bar/15 m^3/h) [58]; C – South African Institute for Advanced Materials Chemistry/University of the Western Cape (2012, 10–200 bar/1 m^3/h) [94]; D – HYSTORSYS AS, Norway (2013, 10–200 bar/10 m^3/h) [188].

pressure), as well as by elimination of possibility of gas contamination by the MH powder. Bowman et al. [193] have conducted extensive cycling tests of Nupro "CW-type" check valves showing no degradation after over 43,000 cycles as well as evaluated porous stainless steel filters to retain hydride powder while allowing sufficient H_2 flow rates.

Suction/H absorption mode of the MH containers/compression elements is provided by the cooling using natural [66,139,179] or forced [133,141] air convection, or flow of cooling fluid (water [62,148,172, etc.] or oil [181,182,184,187]). Some solutions envisage the cooling using a chiller plate [142], or thermoelectric/Peltier modules [96]. To provide high-pressure hydrogen discharge, the MH containers are heated up using electric heaters [66,71,128,133,139,141,142,173–176,179], thermoelectric modules [96], or flow of a heating fluid (hot water at $T_H < 100$ °C [62,135,136,138,148,151,170,171,177,180,181,183], oil [181,182,184–188], overheated water [94,158] or steam [58,94,153] at the higher temperatures). One solution by Ergenics uses heating of the MH containers by the burning of natural gas [134].

The operation of permanently operating MH compressors is usually controlled by time relays which provide a periodic switching of the MH containers between suction/absorption and discharge/desorption modes. As a rule, both absorption and desorption time setpoints are the same that allows to simplify system layout. At the same time, it was noted that in most cases the desorption time is shorter than the absorption one [108,118,126].

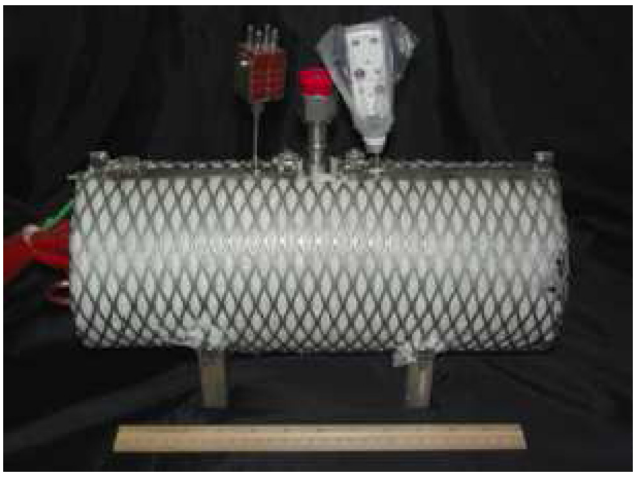

Fig. 18 – A 3-stage metal hydride ($LaNi_{4.5}Al_{0.5}$, $LaNi_{4.9}Al_{0.1}$, and $TiCr_{1.8}$) compressor fabricated at the tritium facility of the Savannah River Site (Aiken SC USA) for compression of hydrogen isotopes to pressures of ~620 bar.

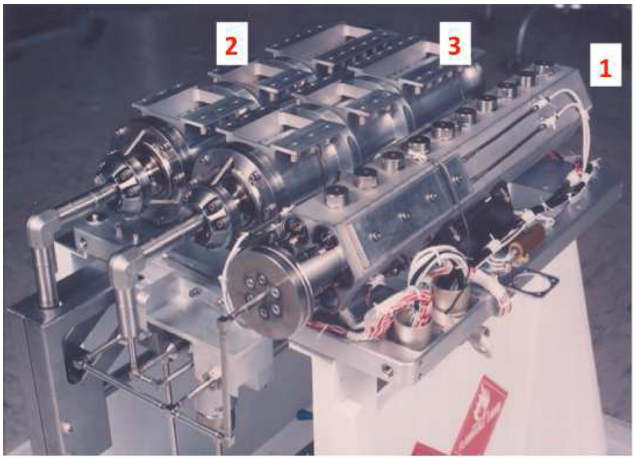

Fig. 19 – JPL 10 K sorption cryocooler hydride compressor bed assembly. (1) Fast absorption hydride bed ($LaNi_{4.8}Sn_{0.2}$); (2) low pressure hydride bed (ZrNi); and (3) high pressure hydride bed ($LaNi_{4.8}Sn_{0.2}$).

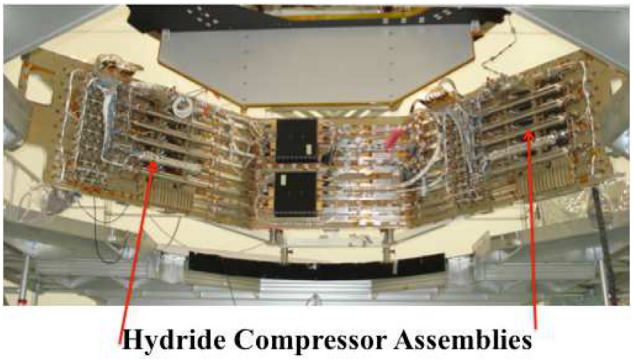

Fig. 20 – Photograph taken during the integration of the hydrogen sorption cryocoolers onto the support structure of the Planck satellite.

It has to be noted that the operating parameters of the MH compressors mostly influence their productivity while the working pressure–temperature ranges are mainly determined by the thermodynamic properties of the selected MH material(s) (see section 2.1). First of all, the productivity depends on the variations of the H_2 suction pressure, cooling temperature, cycle time, and, in a lesser extent, heating temperature and H_2 discharge pressure [94,108]. This influence is especially pronounced in a multistage layout when the combination of the factors specified above mainly affects on hydrogen flow rate between the stages which often becomes a step limiting the total productivity of the compressor [94].

The importance of heat recovery for the increase of MH compressors efficiency was underlined in a number of studies, see, e.g. Refs. [104,106]; the corresponding engineering solutions can be found in patents [189–192]. However, only few system developments known to the authors realise this approach. An attempt to apply the heat recovery by the circulation of water between hot and cold MH containers/compression elements after completion of H_2 absorption–desorption cycle was undertaken by South African co-authors of the present review [94,97]. The solution was shown to be feasible; moreover, its application provided more stable operation of the compressor using water for the cooling and steam for the heating. At the same time, the introduction of the additional circulation loop results in the complication of the system layout and in the increase of its cost. It also results in the decrease of the system productivity.

Examples of medium-to-large scale permanently operated MH compressors are presented in Fig. 17.

3.4. *Applications of MH H_2 compressors*

Since Reilly et al. [62] described a hydride compressor that used VH_x in 1971, a number of possible applications has proposed. Some examples are cited by Sandrock [6,68], Dantzer [7], Bowman and Fultz [11]. However, the most diverse collection of hydride compressors and potential applications can be seen in the literature by Ergenics [81,98–102,133,134,172].

This section briefly presents the most important applications of MH compressors including historical summary, and an overview of the recent developments.

3.4.1. *Isotope handling*

Metal hydrides have been used internationally in the research laboratories, nuclear energy and defence industries for decades to store and process hydrogen isotopes, protium, deuterium, and tritium [194,195]. Prior to 1970 the binary hydrides of titanium, zirconium, palladium, and uranium were only utilised [196]. Often these metal hydrides served concurrent roles of collecting, storing, purifying, transporting, and isotope separation rather than to serve as explicit compression applications. However, several organisations in the U.S. Nuclear Defence industry that included Los Alamos Scientific Laboratory (Alamos NM) [197], the Mound Laboratory (Miamisburg OH) [196] and the Savannah River Site (Aiken SC) [198] generated and supplied highly purified tritium gas at pressures of several bar (typically <5 bar) by heating storage beds of uranium powder to circa 650 K and higher temperatures that can be regarded as a single step MH compressor. There were issues of tritium inventory control and managements due to enhanced permeation of this radioactive gas through the stainless steel bed walls at these elevated temperatures [198,199]. In the mid-1980s, the Savannah River Site (SRS) started the development [200–202] of an enhanced tritium processing facility where several metal hydrides based upon the AB_5 and AB_2 alloys were employed in various roles including as compressors to replace conventional mechanical compressor technology. Using two or three stage compression and different alloys, compression of hydrogen isotopes up to the pressures of 620 bar were achieved for maximum bed temperatures of around 460 K [203]. A photograph of an example 3-stage compressor built at SRS is shown in Fig. 18 where the alloys were $LaNi_{4.5}Al_{0.5}$ (Stage-1 to 14 bar), $LaNi_{4.9}Al_{0.1}$ (Stage-2 to 200 bar), and $TiCr_{1.8}$ (Stage-3 to 620 bar). These compressors provided safe and reliable operation during more than 20 years of their use [203].

Similar development which uses one-stage MH compression for the supply of hydrogen isotopes (hydrogen,

deuterium, tritium, or their mixture) at very high, up to 5 kbar, pressures was reported by Russian Research Institute of Experimental Physics. The periodically operated compression system uses decomposition of vanadium dihydride at $T \leq 360$ °C. It is intended for the use in various experimental studies, including muon-catalysed fusion [179].

3.4.2. *Cryogenics/space*

In 1972, van Mal was the first to report that metal hydride compressors could be used to form liquid hydrogen via Joule–Thomson (J–T) expansion [204,205]. Subsequently, a number of laboratory demonstrations of hydrogen liquefaction using metal hydride compression were done as previously reviewed by Bowman [8,9] and presented in a number of original developments, see, e.g. Refs. [206–208].

A 3-stage hydride compressor was developed and built by a team at NASA Jet Propulsion Laboratory (JPL) and Aerojet Electronic Systems Division (Azusa CA USA) that periodically formed solid molecular hydrogen (s-H_2) at temperatures below 10 K from 100 bar H_2 gas [173] when integrated with a J–T capillary tube and three Stirling cryocoolers operating at $T > 60$ K [174]. The overall H_2 compression ratio from these hydride beds was 8.3×10^5. The hydride compressor assembly is shown in Fig. 19. This cryocooler was operated in earth orbit on-board the Space Shuttle Orbiter Endeavour during May 1996 and successfully generated s-H_2 at 10.4 K on its first cool down cycle [175]. However, small metallic particles that were free floating in the storage volume at zero gravity were swept into control valve preventing J–T valve from fully sealing during subsequent space flight tests [175]. Consequently, only liquid hydrogen at the temperature 18–21 K could be obtained. When these particles were removed from the damaged valve seat at JPL following the space flight, the repaired cryocooler operated normally and was again able to generate s-H_2 at temperatures between 9.4 K and 10.0 K during post-flight tests in the laboratory [175].

Starting from 1997, JPL developed and fabricated two completely redundant 20 K sorption cryocoolers for the European Space Agency (ESA) mission Planck [209] aiming at mapping and measuring the Cosmic Microwave Background (CMB) radiation with higher resolution and sensitivity than any prior study. Comprehensive descriptions of the Planck Mission and the thermal control systems for its satellite are given in Refs. [209,210], respectively. Details on the development and prior-to-launch testing of the sorption cryocoolers and metal hydride (i.e., $LaNi_{4.78}Sn_{0.22}H_x$) compressors are available in Refs. [142,143] and the various papers cited therein. The Planck satellite was launched in May 2009 with the two sorption cryocooler operated in a serial fashion. Excessive degradation in performance of the first unit was noted after less than one year of flight operation and it was switched off. The second flight unit operated within required performance levels for over three years until completion of the Planck flight mission in October 2013. Reasons for this difference are not yet identified, but the extensive flight data files are being reviewed to detect potential causes. Fig. 20 displays the two compressor assemblies being integrated on the support mounting of the Planck satellite. The individual metal hydride beds are mounted onto radiator plates on the outer panels of the satellite. An overview of the performance of the sorption cryocoolers during the first year of space flight operation is given by Ade et al. [211].

3.4.3. *Utilisation of low-grade heat*

As it was already mentioned, the main advantage of MH hydrogen compressors is in the conversion of waste heat ($T < 200$ °C) into the energy of compressed hydrogen which can be further utilised.

In 1979 Nomura et al. [170] developed and successfully tested a piston engine which used one stage MH compressor on the basis of $LaNi_5$ and operated at 20–80 °C providing efficiency of energy conversion of 7.7%, or about 50% of the Carnot efficiency. A year later the first prototype of MH-based ($LaNi_{4.63}Al_{0.37}$) water pump operating in the same temperature range was developed at Sandia National Laboratories [171]. Use of MH compressors for water pumping driven by solar heat was intensively studied in the early 2000s [212–214]. The systems were shown to be promising in distributed stand-

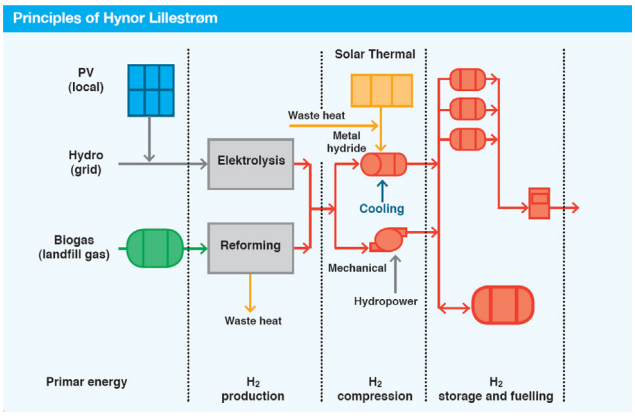

Fig. 21 – Schematics of HyNor Lillestrøm hydrogen refuelling station for FC vehicles.

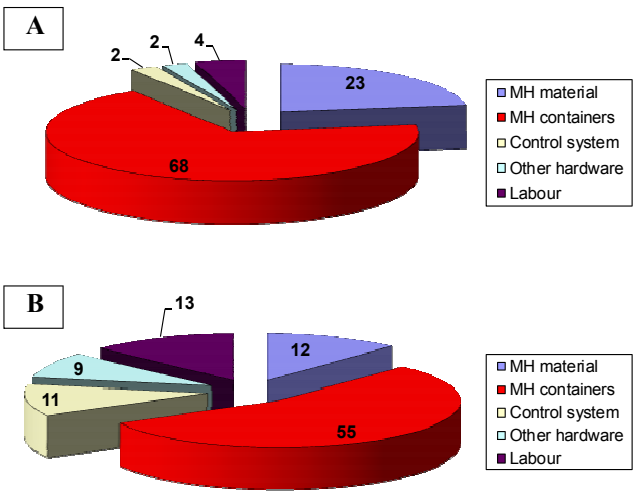

Fig. 22 – Cost breakdown (in %) for prototype MH compressors: A: 10–200 bar/1 m^3/h, South Africa (Fig. 17C); B – 10–200 bar/10 m^3/h, Norway (Fig. 17D; the data were provided by Dr. Jon Eriksen, HYSTORSYS AS). The labour costs relate to system integration only.

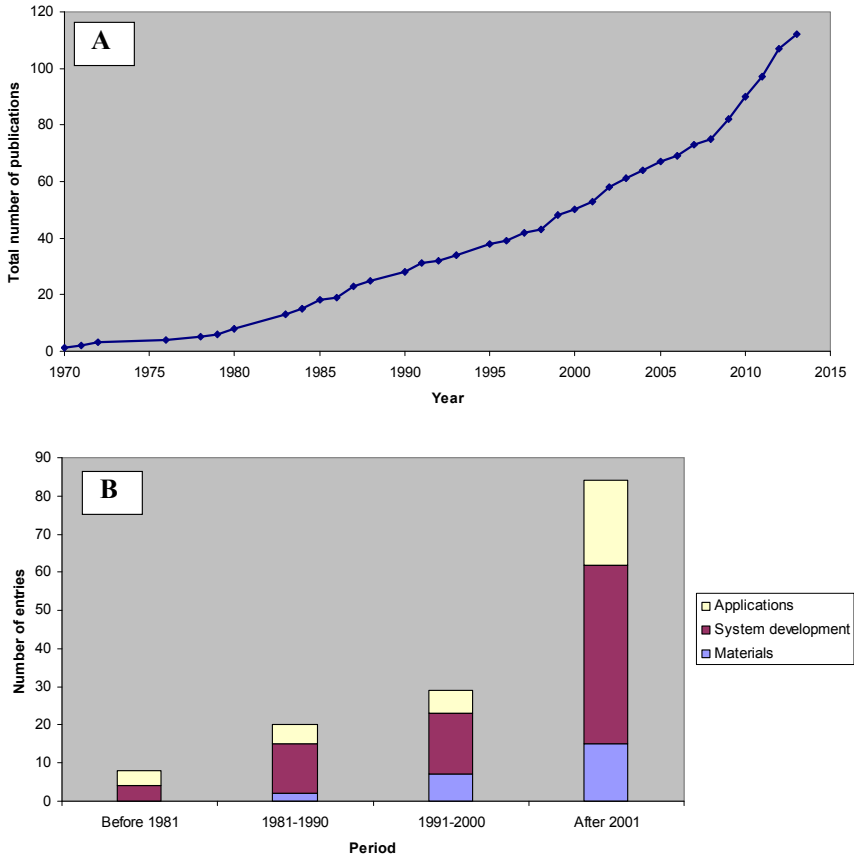

Fig. 23 – Analysis of the reference data on the MH compressors: A – number of publications and patents; B – scope of the work.

alone applications capable of daily pumping up to 3000 L of water over a height of 15 m using 1 m^2 solar collector area [214].

Demonstration of a metal hydride heat engine developed by Ergenics was able to convert the heat from e.g. solar hot water into electricity and can be found in Ref. [215]. The issues of upscaling similar solutions, by integration of MH compressor with radial-axial turbine expansion engine were recently considered by Rusanov et al. [216]. Analysis of performances of energy conversion using MH hydrogen compression in comparison with conventional organic Rankine cycle [217] showed that the MH compression is more promising, due to lower operation cost, higher exergy efficiency and thermal COP, higher output power, and acceptable capital costs. The advantages are especially pronounced for the utilisation of waste industrial heat.

3.4.4. *Thermally driven actuators*

Developments of pneumatic actuators on the basis of MH hydrogen compression were considered in earlier reviews of MH applications [6,68]. Their advantages include compactness, ability to develop high forces, smooth actuation, silent and vibration-free action, simplicity in design and operation. Since the late 1980s Japan Steel Works has carried out intensive R&D of the MH actuators, which were used in various types of rehabilitation equipment [218–220]. As a rule, the actuators are driven by thermoelectric/Peltier elements used for heating and cooling of the MH; pressure transmission from compressed H_2 to mechanical or hydraulic actuating mechanism is provided by bellows. The developed devices have an impressive performance: for example, use of 12 g of $(Ca,Mm)(Ni,Al)_5$ alloy allows to lift 50 kg load by 5 cm [220].

The data about development of MH actuators over last decade can be found in Refs. [220–224] and references therein. The developments are mainly focused on the integration of MH with pneumatic McKibben actuators/"artificial muscles" [222,223], as well as study of feasibility of usage of low-grade (e.g. solar) heat to drive the actuators [224].

3.4.5. *Hydrogen refuelling stations*

Hydrogen refuelling infrastructure takes a significant part of the capital investments for the introducing fuel cell powered vehicles and must be taken into account in the assessment of their economic feasibilities. Despite a certain number of hydrogen refuelling stations operating worldwide, they are not introduced broadly enough, mainly because of their high costs ranging between $500,000 and $5,000,000 per installation [225]. The most expensive H_2 refuelling components originate from: (i) on-site hydrogen production and (ii) hydrogen compression. According to techno-economic analysis presented in Ref. [226], the contribution of hydrogen compression to the total station cost is about 20%.

Cost–performance optimisation of the H_2 refuelling infrastructure can be achieved by the improvement of hydrogen

compression technology. A promising way for that is the application of thermally-driven metal hydride hydrogen compressors characterised by simplicity in design and operation, reliability and minimum maintenance, with potentially low price and ability to utilise waste heat, instead of electricity, for the H_2 compression. An example of the integration of MH compressor in hydrogen refuelling infrastructure is presented in patent [227].

Fig. 21 presents features of the HyNor Lillestrøm hydrogen refuelling station in Norway [228,229]. The station uses on-site produced hydrogen and has three H_2 storage tanks (200, 450 and 1000 bar) on the basis of high-pressure composite cylinders. H_2 compression is carried out using metal hydride (see Fig. 17(D)) and mechanical (membrane) hydrogen compressors. Hydrogen is dispensed to the FC vehicles at the pressure of 700 bar.

3.5. *Economic estimations*

For understandable reasons, the available information about prices for MH hydrogen compressors is scarce. However, there are indications that even the prototype costs for medium-to-large scale MH compressors can be comparable with the prices for commercially available mechanical compressors. So, the estimated cost of the 10–100 bar/0.42 m^3/h prototype built in Brazil [71] was reported as $23,000 versus $27,000 for PPI mechanical compressor (1989). The cost of 3–150 bar/10 m^3/h MH compressor built in Ukraine in 1997 (Fig. 17(A); [141]) was estimated as $32,500–$39,000; the investments could be returned in 5–6 months, due to high price difference between low- and high-pressure hydrogen. The capital costs for 0.5–430 bar MH compressor estimated by Linde North America, MRT and Ergenics in 2009 [136] were about $66,000.

Fig. 22 presents costs breakdown (in %) for the prototype MH compressors recently developed with participation of South African and Norwegian co-authors of this review. It can be seen that the most expensive part of the compressor is metal hydride containers/compression elements, and optimisation of their design and manufacturing technology could result in the significant price decrease.

It is expected that maintenance cost for the MH compressors will be significantly lower than for their mechanical analogues. Thus, the implementation of MH compressors has clear economic advantages.

4. Concluding remarks

Analysis of the reference data summarised in the present review shows a stable growth of the R&D activities in the development of the metal hydride hydrogen compression technology as illustrated by Fig. 23(A) where the total numbers of bibliographic entries explicitly focused on the MH H_2 compression technology are shown. Significant intensification of the R&D on MH hydrogen compressors was observed recently (after 2008) making the present review very timely.

While early works (i.e., during the 1970s–1980s) mainly dealt with the proof of concept and outlining possible applications of the MH compressors on the basis of general features of hydrogen–metal systems, further R&D in this field became more focused, including special research of the MH compression alloys, as well as optimisation of system layout towards improvement of its performances (extension of the operating pressure range, increase of productivity and efficiency, etc.). Many works, especially those published in the last decade, are aimed at the alignment of the material and system features with the requirements of specific applications (Fig. 23(B)[4]).

Commercial competitiveness of the metal hydride compression in comparison with alternative hydrogen compression technologies is justified by both technical and economic considerations.

Use of the waste industrial heat is a major winning argument for use of the MH compression to dramatically decrease its operational costs. Furthermore, costs of the selected MH materials and their availability have a primary importance for a broad application of the technology.

Efficient metal hydride compression process requires

- a high compression ratio (small slope of the isotherms, low hysteresis and appropriate thermodynamics of the metal–hydrogen system);
- high productivity and efficiency (low number of compressions steps, fast kinetics of hydrogen exchange, efficient heat transfer, low transient heat losses);
- long and reliable operation (high cycle stability of metal hydride materials at the operating conditions, efficient system design).

Optimisation of the performances of the MH compressors strongly depends on finding a compromise between a number of contradicting factors, which could be divided into three groups (Table 3).

The first group (A) concerns the development of MH materials for the H_2 compression. These should assure matching specified pressure and available temperature ranges, having maximal reversible sorption capacity, minimal dilatation and heat capacity, in addition to the factors mentioned above in this section. Furthermore, cyclic stability and poisoning resistance of an MH alloy should be taken into account.

The second (B) and third (C) groups of factors are related to the optimisation of the design of the MH compressor, technology of its manufacturing, and operation conditions (i.e. addressing and resolving the engineering problems without adversely impacting system mass/volume values, component manufacturability or assembly, or reliability during long term temperature/pressure cycling).

Finally, successful implementation of metal hydride hydrogen compressors is strongly dependent on their manufacturing costs of which the most expensive items are metal hydride containers/compression elements. Optimisation of the manufacturing will result in the cost

[4] Most of the publications appeared after 1990 have wide scope usually covering various aspects of MH compressor development in one work. That is why the total number of entries specified in Fig. 23(B) exceeds the number of corresponding publications.

Table 3 – Factors influencing the performances of metal hydride hydrogen compressors.

Group	Factor	Performances				
		Suction pressure	Discharge pressure	Efficiency	Productivity	Safety and reliability
A Properties of MH alloy	Entropy of hydride formation, $\|\Delta S^0\|$	Strong increase	Strong increase			
	Enthalpy of hydride formation, $\|\Delta H^0\|$	Strong decrease	Strong decrease	Increase		
	Reversible H sorption capacity, ΔC			Increase	Strong increase	
	Hysteresis, δ_T	Increase	Decrease	Decrease		
	Heat capacity, c		Decrease (for high pressures)	Decrease	Decrease	
	Dilatation, $\Delta V/V_0$			Decrease	Decrease	Strong decrease
	Sorption / desorption kinetics, K_r				Increase	Increase
B Design / technology	Overall heat transfer coefficient, K_H			Increase	Strong increase	
	Overall mass transfer coefficient, K_m				Increase	
	Dead space, K_V			Decrease	Decrease	Strong increase
	Material consumption, K_M			Decrease	Increase	Strong increase
	Heat recovery efficiency, σ			Increase	Decrease	
	Number of stages, n	Decrease	Increase	Decrease	Decrease	Decrease
C Operating conditions	Lower temperature level, T_L	Strong decrease		Decrease	Decrease	
	Upper temperature level, T_H		Strong increase	Increase	Increase	
	Cycle duration, τ_C	Decrease	Increase	Increase	Strong decrease	Increase

reduction and, accordingly, will secure the commercial success of the metal hydride hydrogen compression technology.

Acknowledgements

This invited review written on a request of the Editor-in-Chief of International Journal of Hydrogen Energy, Emre A. Vezir-oğlu, summarises both individual and joint efforts of the co-authors for more than three decades.

Development and characterisation of MH materials for hydrogen compression was done via Program of Research Co-operation between Norway and South Africa funded by Research Council of Norway (RCN) and NRF in South Africa (2007–2010, Project #180344).

Volodymyr A. Yartys greatly acknowledges financial support received from the Research Council of Norway (projects 191106 "Thermally Managed Systems for Storage, Compression and Supply of Hydrogen Gas" and 180200 "Hybrid Hydrogen Storage Solutions"), Hystorsys AS and CMR Prototech. He would like to sincerely thank colleagues from IFE (Dr. Jan Petter Mæhlen), Hystorsys AS (Dr. Jon Eriksen, Dr. Roman V. Denys and Mr. Christoph Cloed) and CMR Prototech (Mr. Arild Vik) for the long standing fruitful collaboration on materials science studies of metal hydrides and on the technologies of hydrogen storage and compression.

Robert C. Bowman, Jr. thanks the Fuel Cell Technology Office of the U.S. Department of Energy, Office of Energy Efficiency and Renewable Energy for their support of his work at the Oak Ridge National Laboratory. He also thanks Dr. Ted Motyka for providing information on the hydride compressor technology at the Savannah River Site and Prof. Ted B. Flanagan for more than two decades of fruitful collaborations on properties of metal hydrides. He also greatly appreciates the contributions made by his numerous colleagues at the Jet Propulsion Laboratory during the development of the hydrogen sorption cryocoolers. This manuscript has been authored by UT-Battelle, LLC, under Contract No. DE-AC05-00OR22725 with the U.S. Department of Energy. The United States Government retains and the publisher, by accepting the article for publication, acknowledges that the United States Government retains a non-exclusive, paid-up, irrevocable, world-wide license to publish or reproduce the published form of this manuscript, or allow others to do so, for United States Government purposes.

Mykhaylo Lototskyy and Bruno G. Pollet, would like to acknowledge support of Eskom Holdings Ltd (South Africa) who mainly funded the developments of MH hydrogen compressors at South African Institute for Advanced Materials Chemistry (SAIAMC). The invaluable contribution of the Department of Science and Technology (DST) in South Africa within a number of Research, Development and Innovation programmes and projects, including Hydrogen South Africa National Flagship Programme (HySA), is greatly acknowledged. The R&D activities in the development and optimisation of MH hydrogen compressors were also supported by Impala Platinum Ltd (South Africa). Investments from the industrial funders have been leveraged through the Technology and Human Resources for Industry Programme, jointly managed by the South African National Research Foundation and the Department of Trade and Industry (NRF/DTI; THRIP projects TP2010071200039, TP2011070800020, and TP1207254249). Mykhaylo Lototskyy also acknowledges NRF support via incentive funding grant 76735.

Finally, Mykhaylo Lototskyy would like to thank a metal hydride team from the Institute for Mechanical Engineering Problems of the National Academy of Sciences of Ukraine (now Hydrogen Power Engineering Department), where he was working for 20 years and contributed to the generation of numerous R&D outputs part of which was analysed in this review. Sincere personal gratitude is addressed to the team leader, Professor V.V.Solovey, as well as to the memory of late team members, Yuri Shmal'ko (1948–2008) and Alexander Ivanovsky (1954–2013).

REFERENCES

[1] Lynch JF, Maeland AJ, Libowitz GG. Hydrogen compression by metal hydrides. In: Veziroglu TN, Taylor IB, editors. Hydrogen energy progress V. Proc. 5th world hydrogen energy conference, vol. 1. Oxford: Pergamon Press; 1984. pp. 1327–37.

[2] Dantzer P, Orgaz E. Thermodynamics of the hydride chemical heat pump: model (I). J Chem Phys 1986;85:2961–73.

[3] Dantzer P, Orgaz E. Thermodynamics of hydride chemical heat pump: II. How to select a pair of alloys. Int J Hydrogen Energy 1986;11:797–806.

[4] Orgaz E, Dantzer P. Thermodynamics of the hydride chemical heat pump: III. Considerations for multistage operation. J Less-Common Met 1987;131:385–98.

[5] Solovey VV. Metal hydride thermal power installations. In: Veziroglu TN, Protsenko AN, editors. Hydrogen energy progress VII. Proc. 7th world hydrogen energy conference, vol. 2. Oxford: Pergamon Press; 1988. pp. 1391–9.

[6] Sandrock G. Applications of hydrides. In: Yurum Y, editor. Hydrogen energy system. Production and utilization of hydrogen and future aspects. Kluwer Acad Publ. NATO ASI Ser. Ser E, 295; 1995. pp. 253–80.

[7] Dantzer P. Metal-hydride technology: a critical review. In: Wipf H, editor. Hydrogen in metals III. Properties and applications. Berlin-Heidelberg: Springer-Verlag; 1997. pp. 279–340.

[8] Bowman Jr RC, Kiehl B, Marquardt E. Closed-cycle Joule-Thomson cryocoolers. In: Donabedian M, editor. Spacecraft thermal control handbook. Cryogenics, vol. 2. El Segundo, CA, USA: The Aerospace Press; 2003. pp. 187–216.

[9] Bowman Jr RC. Development of metal hydride beds for sorption cryocoolers in space applications. J Alloys Compds 2003;356–357:789–93.

[10] Muthukumar P, Groll M. Erratum to "metal hydride based heating and cooling systems: a review" [International Journal of Hydrogen Energy (2010) 35: 3817–3831]. Int J Hydrogen Energy 2010;35. 8816–8829*. * The authors [10] recommend to refer to the Erratum since the original article contains several publisher's errors corrected in the second version.

[11] Bowman RC, Fultz B. Metallic hydrides I: hydrogen storage and other gas-phase applications. MRS Bull 2002;27(9):688–93.

[12] Tarasov BP, Lototskii MV, Yartys' VA. Problem of hydrogen storage and prospective uses of hydrides for hydrogen accumulation. Russ J Gen Chem 2007;77(4):694–711.

[13] Flanagan TB, Oates WA. Thermodynamics of intermetallic compound–hydrogen systems. In: Schlapbach L, editor. Hydrogen in intermetallic compounds. I. Electronic, thermodynamic and crystallographic properties, preparation. Berlin–Heidelberg; 1988. pp. 49–85.

[14] Sandrock G. Hydrogen–metal systems. In: Yurum Y, editor. Hydrogen energy system. Production and utilization of hydrogen and future aspects. Kluwer Acad Publ. NATO ASI Ser. Ser E, 295; 1995. pp. 135–66.

[15] Lototsky MV, Yartys VA, Zavaliy IYu. Vanadium-based BCC alloys: phase-structural characteristics and hydrogen sorption properties. J Alloys Compds 2005;404–406:421–6.

[16] Kodama T. The thermodynamic parameters for the $LaNi_{5-x}Al_x$–H and $MmNi_{5-x}Al_x$–H systems. J Alloys Compds 1999;289:207–12.

[17] Khyzhun OYu, Lototsky MV, Riabov AB, Rosenkilde C, Yartys VA, Jørgensen S, et al. Sn-containing (La,Mm) $Ni_{5-x}Sn_xH_{5-6}$ intermetallic hydrides: thermodynamic, structural and kinetic properties. J Alloys Compds 2003;356–357:773–8.

[18] Dehouche Z, Grimard N, Laurencelle F, Goyette J, Bose TK. Hydride alloys properties investigations for hydrogen sorption compressor. J Alloys Compds 2005;399:224–36.

[19] Luo S, Luo W, Clewley JD, Flanagan TB, Bowman RC. Thermodynamic and degradation studies of $LaNi_{4.8}Sn_{0.2}$–H using isotherms and calorimetry. J Alloys Compds 1995;231:473–8.

[20] Dantzer P, Meuner F. What materials to use in hydride chemical heat pumps. Mat Sci Forum 1988;31:1–18.

[21] Diaz H, Percheron-Guegan A, Achard JC. Thermodynamic and structural properties of $LaNi_{5-y}Al_y$ compounds and their related hydrides. Int J Hydrogen Energy 1979;4:445–54.

[22] Singh RK, Gupta BK, Lototsky MV, Srivastava ON. On the synthesis and hydrogenation behaviour of $MmNi_{5-x}Fe_x$ alloys and computer simulation of their P–C–T curves. J Alloys Compds 2004;373:208–13.

[23] Libowitz GG, Maeland AJ. Use of vanadium-based solid solution alloys in metal hydride heat pumps. J Less-Common Met 1987;131:275–82.

[24] Huston EL, Sandrock GD. Engineering properties of metal hydrides. J Less-Common Met 1985;74:435–43.

[25] Luo G, Chen JP, Li SL, Chen W, Han XB, Chen DM, et al. Properties of $La_{0.2}Y_{0.8}Ni_{5-x}Mn_x$ alloys for high-pressure hydrogen compressor. Int J Hydrogen Energy 2010;35:8262–7.

[26] Kapischke J, Hapke J. Measurement of the pressure-composition isotherms of high-temperature and low-temperature metal hydrides. Exper Therm Fluid Sci 1998;18:70–81.

[27] Guo X, Wang S, Liu X, Li Z, Lü F, Mi J, et al. Laves phase hydrogen storage alloys for super-high-pressure metal hydride hydrogen compressors. Rare Met 2011;30(3):227–31.

[28] Wang X, Chen R, Zhang Y, Chen C, Wang Q. Hydrogen storage properties of (La–Ce–Ca)Ni_5 alloys and application for hydrogen compression. Mater Lett 2007;61:1101–4.

[29] Au M, Wang Q. Rare earth-nickel alloy for hydrogen compression. J Alloys Compds 1993;201:115–9.

[30] Zotov TA, Sivov RB, Movlaev EA, Mitrokhin SV, Verbetsky VN. IMC hydrides with high hydrogen dissociation pressure. J Alloys Compds 2011;509S:S839–43.

[31] Johnson JR. Reaction of hydrogen with the high temperature (C14) form of $TiCr_2$. J Less-Common Met 1980;73:345–54.

[32] Wang X, Chen R, Zhang Y, Chen C, Wang Q. Hydrogen storage alloys for high-pressure suprapure hydrogen compressor. J Alloys Compds 2006;420:322–5.

[33] Brodowsky H, Yasuda K, Itagaki K. From partition function to phase diagram–statistical thermodynamics of the $LaNi_5$–H system. Z Phys Chem 1993;179:45–55.

[34] Beeri O, Cohen D, Gavra Z, Johnson JR, Mintz MH. Thermodynamic characterization and statistical thermodynamics of the TiCrMn–H (D) system. J Alloys Compds 2000;299:217–26.

[35] Shilov AL, Efremenko NE. Effect of sloping pressure "plateau" in two-phase regions of hydride systems. Russ J Phys Chem 1986;60:3024–8.

[36] Larsen JW, Livesay BR. Hydriding kinetics of $SmCo_5$. J Less-Common Met 1980;73:79–88.

[37] Fujitani S, Nakamura H, Furukawa A, Nasako K, Satoh K, Imoto T, et al. A method for numerical expressions of P-C isotherms of hydrogen-absorbing alloys. Z Phys Chem 1993;179:27–33.

[38] Lototsky MV. A modification of the Lacher–Kierstead theory for simulation of PCT diagrams of real "hydrogen–hydride-forming material" systems. Kharkov Univ Bull/No. 477: Chem Ser 2000;5(28):45–53.

[39] Lototsky MV, Yartys VA, Marinin VS, Lototsky NM. Modelling of phase equilibria in metal–hydrogen systems. J Alloys Compds 2003;356–357:27–31.

[40] Park CN, Luo S, Flanagan TB. Analysis of sloping plateaux in alloys and intermetallic hydrides. I. Diagnostic features. J Alloys Compds 2004;384:203–7.
[41] Lacher JR. A theoretical formula for the solubility of hydrogen in palladium. Proc Roy Soc (Lond) 1937;A161:525–45.
[42] Kierstead HA. A theory of multiplateau hydrogen absorption isotherms. J Less-Common Met 1980;71:303–9.
[43] Flanagan TB, Clewley JD. Hysteresis in metal hydrides. J Less-Common Met 1982;83:127–41.
[44] Balasubramaniam R. Hysteresis in metal–hydrogen systems. J Alloys Compds 1997;253–254:203–6.
[45] Murthy SS. Heat and mass transfer in solid state hydrogen storage: a review. J Heat Transf 2012;134:031020.
[46] Golubkov AN, Yuhimchuk AA. Sources of high pressure hydrogen isotopes. J Mosc Phys Soc 1999;9(3):223–31.
[47] Goodell PD. Thermal conductivity of hydriding alloy powders and comparisons of reactor systems. J Less-Common Met 1980;74:175–84.
[48] Sandrock G. A panoramic overview of hydrogen storage alloys from a gas reaction point of view. J Alloys Compds 1999;293–295:877–88.
[49] Førde T, Maehlen JP, Yartys VA, Lototsky MV, Uchida H. Influence of intrinsic hydrogenation/dehydrogenation kinetics on the dynamic behaviour of metal hydrides: a semi-empirical model and its verification. Int J Hydrogen Energy 2007;32:1041–9.
[50] Førde T, Næss E, Yartys VA. Modelling and experimental results of heat transfer in a metal hydride store during hydrogen charge and discharge. Int J Hydrogen Energy 2009;34:5121–30.
[51] Bloch J, Mintz MH. Kinetics and mechanisms of metal hydride formation – a review. J Alloys Compds 1997;253:529–41.
[52] Corré S, Bououdina M, Fruchart D, Adachi G. Stabilisation of high dissociation pressure hydrides of formula $La_{1-x}Ce_xNi_5$ ($x = 0–0.3$) with carbon monoxide. J Alloys Compds 1998;275–277:99–104.
[53] Goodell PD. Stability of rechargeable hydriding alloys during extended cycling. J Less Common Met 1984;99:1–14.
[54] Park JM, Lee JY. The intrinsic degradation phenomena of $LaNi_5$ and $LaNi_{4.7}Al_{0.3}$ by temperature induced hydrogen absorption-desorption cycling. Mat Res Bull 1987;22:455–65.
[55] Shen CC, Perng TP. On the cyclic hydrogenation stability of an $Lm(NiAl)_5$-based alloy with different hydrogen loadings. J Alloys Compds 2005;392:187–91.
[56] Cheng HH, Yang HG, Li SL, Deng XX, Chen DM, Yang K. Effect of hydrogen absorption/desorption cycling on hydrogen storage performance of $LaNi_{4.25}Al_{0.75}$. J Alloys Compd 2008;453:448–52.
[57] Baichtok YuK, Mordkovich VZ, Dudakova NV, Avetisov AK, Kasimtsev AV, Mordovin VP. Technological possibilities and state of the art in the development of hydride thermal sorption hydrogen compressors. Int Sci J Altern Energy Ecol (ISJAEE) 2004;2(10):50–4.
[58] Bocharnikov MS, Yanenko YuV, Tarasov BP. Metal hydride thermosorption compressor of hydrogen high pressure. Int Sci J Altern Energy Ecol ISJAEE 2012;12(116):18–23.
[59] Shilov AL, Padurets LN, Kost ME. Thermodynamics of hydrides of intermetallic compounds of transition metals. Russ J Phys Chem 1985;59(8):1857–75.
[60] Griessen R, Driessen A, De Groot DG. Search for new metal-hydrogen systems for energy storage. J Less-Common Met 1984;103:235–44.
[61] Cantrell JS, Bowman Jr RC, Attalla A, Baker RW. Studies of phase compositions and hydrogen diffusion in VH_x. Z Phys Chem NF 1993;181:83–8.
[62] Reilly JJ, Holtz A, Wiswall Jr RH. A new laboratory gas circulation pump for intermediate pressures. Rev Sci Instr 1971;42:1485–6.
[63] Bowman Jr RC, Freeman BD, Phillips JR. Evaluation of metal hydride compressors for applications in Joule-Thomson cryocoolers. Cryogenics 1992;32:127–38.
[64] Lynch JF, Maeland AJ, Libowitz GG. The vanadium-rich V–Ti–Fe/H_2 system. Z Phys Chem 1985;145:51–9.
[65] Bowman RC, Lynch FE, Marmaro RW, Luo CH, Fultz B, Cantrell JS, Chandra D, et al. Effects of thermal cycling on the physical properties of VH_x. Z Phys Chem 1993;181:269–73.
[66] Wiswall RH, Reilly JJ. Method of storing hydrogen. Patent US3516263, 1970.
[67] Williams M, Lototsky MV, Davids MW, Linkov V, Yartys VA, Solberg JK. Chemical surface modification for the improvement of the hydrogenation kinetics and poisoning resistance of TiFe. J Alloys Compds 2011;509S:770–4.
[68] Sandrock G, Suda S, Schlapbach L. Applications. In: Schlapbach L, editor. Hydrogen in intermetallic compounds. II. Surface and dynamic properties, applications. Berlin – Heidelberg; 1992. pp. 197–258.
[69] Lototsky MV, Williams M, Yartys VA, Klochko YeV, Linkov VM. Surface-modified advanced hydrogen storage alloys for hydrogen separation and purification. J Alloys Compds 2011;509S:S555–61.
[70] Modibane KD, Williams M, Lototskyy M, Davids MW, Klochko Ye, Pollet BG. Poisoning-tolerant metal hydride materials and their application for hydrogen separation from CO_2/CO containing gas mixtures. Int J Hydrogen Energy 2013;38:9800–10.
[71] Da Silva EP. Industrial prototype of a hydrogen compressor based on metallic hydride technology. Int J Hydrogen Energy 1993;18(4):307–11.
[72] Liu FJ, Suda S. A method for improving the long-term storability of hydriding alloys by air/water exposure. J Alloys Compds 1995;231:411–6.
[73] Uchida H. Surface properties of H_2 on rare earth based hydrogen storage alloys with various surface modifications. Int J Hydrogen Energy 1999;24:861–9.
[74] Golben PM. Passive purification in metal hydride storage apparatus. Patent US 6508866 B1, 2003.
[75] Hu X, Qi Z, Yang M, Chen J. A 38 MPa compressor based on metal hydrides. J Shanghai Jiaotong Univ (Sci) 2012;17(1):53–7.
[76] Friedlmeier G, Manthey A, Wanner M, Groll M. Cyclic stability of various application-relevant metal hydrides. J Alloys Compds 1995;231:880–7.
[77] Wanner M, Friedlmeier G, Hoffmann G, Groll M. Thermodynamic and structural changes of various intermetallic compounds during extended cycling in closed systems. J Alloys Compds 1997;253–254:692–7.
[78] Bowman Jr RC, Payzant EA, Wilson PR, Pearson DP, Ledovskikh A, Danilov D, et al. Characterization and analyses of degradation and recovery of $LaNi_{4.78}Sn_{0.22}$ hydrides following thermal aging. J Alloys Compds 2013;580S:S207–10.
[79] Iosub V, Joubert JM, Latroche M, Černy R, Percheron-Guegan A. Hydrogen cycling induced peak broadening in C14 and C15 laves phases. J Sol St Chem 2005;178:1799–806.
[80] Park JG, Kim DM, Jang KJ, Han JS, Cho K, Lee JY. The intrinsic degradation behaviour of $(V_{0.53}Ti_{0.47})_{0.925}Fe_{0.075}$ alloy during temperature-induced hydrogen absorption-desorption cycling. J Alloys Compds 1999;293–295:150–5.
[81] Golben M, DaCosta DH. Disproportionation resistant alloy development for hydride hydrogen compression. Proc 2002 U.S. DOE Hydrogen Program Review NREL/CP-610-32405.
[82] Bowman RC, Lindensmith CA, Luo S, Flanagan TB, Vogt T. Degradation behavior of $LaNi_{5-x}Sn_xH_z$ ($x = 0.20–0.25$) at

elevated temperatures. J Alloys Compds 2002;330–332:271–5.
[83] Prina M, Bowman RC, Kulleck JG. Degradation study of $ZrNiH_{1.5}$ for use as actuators in gas gap heat switches. J Alloys Compds 2004;373:104–14.
[84] Reiter JW, Karlmann PB, Bowman RC, Prina M. Performance and degradation of gas-gap heat switches in hydride compressor beds. J Alloys Compds 2007;446–447:713–7.
[85] Laurencelle F, Dehouche Z, Goyette J. Hydrogen sorption cycling performance of $LaNi_{4.8}Sn_{0.2}$. J Alloys Compds 2006;424:266–71.
[86] Li SL, Chen W, Chen DM, Yang K. Effect of long-term hydrogen absorption/desorption cycling on hydrogen storage properties of $MmNi_{3.55}Co_{0.75}Mn_{0.4}Al_{0.3}$. J Alloys Compds 2009;474:164–8.
[87] Li SL, Chen W, Luo G, Han XB, Chen DM, Yang K, et al. Effect of hydrogen absorption/desorption cycling on hydrogen storage properties of a $LaNi_{3.8}Al_{1.0}Mn_{0.2}$ alloy. Int J Hydrogen Energy 2012;37:3268–75.
[88] Crivello JC, Gupta M. Electronic properties of $LaNi_{4.75}Sn_{0.25}$, $LaNi_{4.5}M_{0.5}$ (M = Si, Ge, Sn), $LaNi_{4.5}Sn_{0.5}H_5$. J Alloys Compds 2003;356–357:151–5.
[89] Mordkovich VZ, Baichtok YuK, Korostyshevsky NN, Sosna MH. Chemical compression of hydrogen up to 40 MPa: problems of materials and design. In: Block DL, Veziroglu TN, editors. Hydrogen energy progress. X. Proc. 10th world hydrogen energy Conf. Cocoa Beach, Florida, USA, 20–24 June 1994, vol. 2. Oxford: Pergamon Press; 1994. pp. 1029–38.
[90] Smith KC, Fisher TS. Models for metal hydride particle shape, packing, and heat transfer. Int J Hydrogen Energy 2012;37:13417–28.
[91] Nasako K, Ito Y, Hiro N, Osumi M. Stress on a reaction vessel by the swelling of a hydrogen absorbing alloy. J Alloys Compds 1998;264:271–6.
[92] Yartys VA, Denys RV, Webb CJ, Mæhlen JP, MacA Gray E, et al. High pressure *in situ* diffraction studies of metal–hydrogen systems. J Alloys Compds 2011;509S:S817–22.
[93] Riabov AB, Denys RV, Maehlen JP, Yartys VA. Synchrotron diffraction studies and thermodynamics of hydrogen absorption–desorption processes in $La_{0.5}Ce_{0.5}Ni_4Co$. J Alloys Compds 2011;509S:S844–8.
[94] Lototskyy M, Klochko Ye, Linkov V, Lawrie P, Pollet BG. Thermally driven metal hydride hydrogen compressor for medium-scale applications. Energy Procedia 2012;29:347–56.
[95] Charlas B, Gillia O, Doremus P, Imbault D. Experimental investigation of the swelling/shrinkage of a hydride bed in a cell during hydrogen absorption/desorption cycles. Int J Hydrogen Energy 2012;37:16031–41.
[96] Yartys V, Lototskyy M, Maehlen JP, Halldors H, Vik A, Strandm A. Continuously-operated metal hydride hydrogen compressor, and method of operating the same. Patent application WO 2010/087723 A1, 2010.
[97] Lototskyy M, Klochko Ye, Linkov VM. Metal hydride hydrogen compressor. Patent application WO 2012/114229 Al, 2012.
[98] Golben PM. Multi-stage hydride-hydrogen compressor. In: Proceedings of the eighteenth intersociety energy conversion engineering conference, Orlando, FL, August 21–26, 1983. Volume 4 (A84-30169 13-44). New York: American Institute of Chemical Engineers; 1983. pp. 1746–53.
[99] DaCosta DH. Advanced thermal hydrogen compression. Proc 2000 hydrogen program review, NREL/CP-570-28890.
[100] Golben PM, Rosso MJ. Hydrogen compressor. Patent US 4402187, 1983.
[101] Golben PM, Rosso MJ. Hydrogen compressor. Patent Application EP0094202 A2, 1983.
[102] Golben PM. Hydrogen compressor. Patent US 4505120, 1985.
[103] Solovey VV. Metal hydride energy-technological hydrogen processingIn Reports of Ukrainian Academy of Science, series A, 3; 1983. pp. 77–80.
[104] Solovey VV, Ivanovsky AI, Chernaya NA, Shevchenko AA. Energy saving technologies for the generation and energy-technological processing of hydrogen. Kompressornoe energeticheskoe mashinostroenie (Compress Energy Eng) 2010;2(20):21–4.
[105] Popovich VA, Ivanovsky AI, Solovey VV, Makarov AA. Thermal sorption compressor for power installationIn VANT (Probl. in nuclear science and engineering, ser. nuclear-hydrogen energy and technology), 3; 1987. pp. 56–8.
[106] Mordkovich VZ, Baichtok YuK, Sosna MKh, Dudakova NV, Korostyshevsky NN. Efficiency analysis for use of intermetallic compounds in hydrogen isolation and compression. Teor Osn Khimicheskoi tekhnologii (Found Chem Technol) 1990;24(6):769–74.
[107] In'kov AP, Popovich VA, Komyanko IS. Effect of the constructional parameters of thermosorption compressors on the efficiency of the compression process. Chem Petrol Eng 1991;26(7–8):363–6.
[108] Muthukumar P, Prakash Maiya M, Srinivasa Murthy S. Parametric studies on a metal hydride based single stage hydrogen compressor. Int J Hydrogen Energy 2002;27:1083–92.
[109] Hopkins RR, Kim KJ. Hydrogen compression characteristics of a dual stage thermal compressor system utilizing $LaNi_5$ and $Ca_{0.6}Mm_{0.4}Ni_5$ as the working metal hydrides. Int J Hydrogen Energy 2010;35:5693–702.
[110] Kelly NA, Girdwood R. Evaluation of a thermally-driven metal-hydride-based hydrogen compressor. Int J Hydrogen Energy 2012;37:10898–916.
[111] RIX Industries (www.rixindustries.com), RIX 3KX series compressors.
[112] Isselhorst A. Heat and mass transfer in coupled hydride reaction beds. J Alloys Compds 1995;231:871–9.
[113] Askri F, Jemni A, Ben Nasrallah S. Dynamic behavior of metal–hydrogen reactor during hydriding process. Int J Hydrogen Energy 2004;29:635–47.
[114] Zhang J, Fisher TS, Ramachandran PV, Gore JP, Mudawar I. A review of heat transfer issues in hydrogen storage technologies. J Heat Transf 2005;127:1391–9.
[115] Wang Y, Adroher XC, Chen J, Yang XG, Miller T. Three-dimensional modeling of hydrogen sorption in metal hydride hydrogen storage beds. J Power Sources 2009;194:997–1006.
[116] Ghafir MFA, Batcha MFM, Raghavan VR. Prediction of the thermal conductivity of metal hydrides – the inverse problem. Int J Hydrogen Energy 2009;34:7125–30.
[117] Krokos CA, Nikolic D, Kikkinides ES, Georgiadis MC, Stubos AK. Modeling and optimization of multi-tubular metal hydride beds for efficient hydrogen storage. Int J Hydrogen Energy 2009;34:9128–40.
[118] Wang Y, Yang F, Meng X, Guo Q, Zhang Z, Park IS, et al. Simulation study on the reaction process based single stage metal hydride thermal compressor. Int J Hydrogen Energy 2010;35:321–8.
[119] Melnichuk M, Silin N, Andreasen G, Corso HL, Visintin A, Peretti HA. Hydrogen discharge simulation and testing of a metal-hydride container. Int J Hydrogen Energy 2010;35:5855–9.
[120] Yang FS, Wang GX, Zhang ZX, Rudolph V. Investigation on the influences of heat transfer enhancement measures in a thermally driven metal hydride heat pump. Int J Hydrogen Energy 2010;35:9725–35.
[121] Muthukumar P, Venkata Ramana S. Study of heat and mass transfer in $MmNi_{4.6}Al_{0.4}$ during desorption of hydrogen. Int J Hydrogen Energy 2010;35:10811–8.

[122] Bhouri M, Goyette J, Hardy BJ, Anton DL. Honeycomb metallic structure for improving heat exchange in hydrogen storage system. Int J Hydrogen Energy 2011;36:6723–38.

[123] Talagañis BA, Meyer GO, Aguirre PA. Modeling and simulation of absorption–desorption cyclic processes for hydrogen storage-compression using metal hydrides. Int J Hydrogen Energy 2011;36:13621–31.

[124] Wang H, Prasad AK, Advani SG. Hydrogen storage systems based on hydride materials with enhanced thermal conductivity. Int J Hydrogen Energy 2012;37:290–8.

[125] Garrison SL, Hardy BJ, Gorbounov MB, Tamburello DA, Corgnale C, vanHassel BA, et al. Optimization of internal heat exchangers for hydrogen storage tanks utilizing metal hydrides. Int J Hydrogen Energy 2012;37:2850–61.

[126] Visaria M, Mudawar I. Experimental investigation and theoretical modeling of dehydriding process in high-pressure metal hydride hydrogen storage systems. Int J Hydrogen Energy 2012;37:5735–49.

[127] Baichtok YK, Avetisov AK, Baranov YM, Telyashev RG, Mordkovich VZ, Suvorkin SV, et al. Shell and tube module for a hydride thermosorption hydrogen separator and compressor. Patent Application WO 2013/006091 A1 (PCT/RU20121000522).

[128] Lototsky M, Halldors H, Klochko Ye, Ren J, Linkov V. 7–200 bar/60 L/h continuously operated metal hydride hydrogen compressor. In: Schur DV, Zaginaichenko SYu, Veziroglu TN, Skorokhod VV, editors. Hydrogen materials science and chemistry of carbon nanomaterials: ICHMS'2009 XI Int Conf, Yalta – Crimea – Ukraine, August 25–31, 2009. Kiev: AHEU Publ.; 2009. pp. 298–9.

[129] Golben PM. Thermally reversible heat exchange unit and method of using same. Patent US 4687049, 1987.

[130] Golben PM. Thermally reversible heat exchange unit. Patent US 4782146, 1988.

[131] Voss MG, Stevenson JR, Mross GA. Hydrogen storage and release device. Patent US 7455723 B2; 2008.

[132] Golben PM, Fox JE. Modular manifold gas delivery system. Patent US 5623987, 1997.

[133] Golben M, DaCosta DH. Advanced thermal hydrogen compression. Proc 2001 hydrogen program review; NREL/CP-570-30535.

[134] DaCosta DH, Golben M. Hydride based hydrogen compression. US DOE hydrogen and fuel cells program 2004: annual Merit review, www.hydrogen.energy.gov/pdfs/review04/hpd_p13_dacosta.pdf; May 26, 2004; FY 2004 Progress Report; http://www.hydrogen.energy.gov/pdfs/progress04/iih1_dacosta.pdf.

[135] Tamhankar S, Boyd T, Gulamhusein A, Golben M, DaCosta D. Integrated hydrogen production, purification and compression system. DoE hydrogen program, project PD7, http://www.hydrogen.energy.gov/pdfs/review08/pd_7_tamhankar.pdf; June 10, 2008.

[136] Tamhankar S, Boyd T, Gulamhusein A, Golben M, DaCosta D. Integrated hydrogen production, purification and compression system. DoE hydrogen program, project PDP29, http://www.hydrogen.energy.gov/pdfs/review09/pdp_29_tamhankar.pdf; May 19, 2009.

[137] Lototsky M, Linkov VM. Hydride container. Patent ZA 2009/02427, 2010.

[138] Laurencelle F, Dehouche Z, Goyette J, Bose TK. Integrated electrolyser –metal hydride compression system. Int J Hydrogen Energy 2006;31:762–8.

[139] Solovey VV, Ivanovsky AI, Kolosov VI, Shmal'ko YuF. Series of metal hydride high pressure hydrogen compressors. J Alloys Compds 1995;231:903–6.

[140] Ivanovsky AI, Kolosov VI, Lototsky MV, Solovey VV, Shmal'ko YF, Kennedy LA. Metal hydride thermosorption compressors with improved dynamic characteristics. Int J Hydrogen Energy 1996;21:1053–5.

[141] Shmal'ko YuF, Ivanovsky AI, Lototsky MV, Kolosov VI, Volosnikov DV. Sample pilot plant of industrial metal-hydride compressor. Int J Hydrogen Energy 1999;24:645–8.

[142] Pearson D, Bowman R, Prina M, Wilson P. The Planck sorption cooler: using metal hydrides to produce 20K. J Alloys Compds 2007;446–447:718–22.

[143] Morgante G, Pearson D, Melot F, Stassi P, Terenzi L, Wilson P, et al. Cryogenic characterization of the Planck sorption cooler system flight model. JINST 2009;4:T12016. http://iopscience.iop.org/1748-0221/4/12/T12016.

[144] Halene C. Method and apparatus for compressing hydrogen gas, Patent US 4995235, 1991.

[145] Ovshinsky SR, Young RT, Li Y, Myasnikov V, Sobolev V. Hydrogen storage bed system including an integrated thermal management system. Patent US 6833118 B2, 2004.

[146] Ovshinsky SR, Young RT, Li Y, Myasnikov V, Sobolev V, Bavarian F. Hydrogen storage bed system including an integrated thermal management system. Patent US 6878353 B2, 2005.

[147] Souahlia A, Dhaou H, Askri F, Sofiene M, Jemni A, Ben Nasrallah S. Experimental and comparative study of metal hydride hydrogen tanks. Int J Hydrogen Energy 2011;36:12918–22.

[148] Nomura K, Akiba E, Ono S. Development of a metal hydride compressor. J Less-Common Met 1983;89:551–8.

[149] Sun DW. Designs of metal hydride reactors. Int J Hydrogen Energy 1992;17:945–9.

[150] Stetson NT, Marchio M, Holland A, Alper D, Gorman D, Yang J. Vane heat transfer structure. Patent US 6626323 B2, 2003.

[151] Muthukumar P, Prakash Maiya M, Srinivasa Murthy S. Experiments on a metal hydride based hydrogen compressor. Int J Hydrogen Energy 2005;30:879–92.

[152] Souahlia A, Dhaou H, Askri F, Mellouli S, Jemni A, Ben Nasrallah S. Experimental study and characterization of metal hydride containers. Int J Hydrogen Energy 2011;36:4952–7.

[153] Astanovsky DL, Astanovsky LZ, Verteletsky PV. Adsorption compression device. Patent RU 2439368 C1, 2012.

[154] Mellouli S, Dhaou H, Askri F, Jemni A, Ben Nasrallah S. Hydrogen storage in metal hydride tanks equipped with metal foam heat exchanger. Int J Hydrogen Energy 2009;34:9393–401.

[155] Tsai ML, Yang TS. On the selection of metal foam volume fraction for hydriding time minimization of metal hydride reactors. Int J Hydrogen Energy 2010;35:11052–63.

[156] Kim KJ, Feldman KT, Lloyd G, Razani A, Shanahan KL. Performance of high power metal hydride reactors. Int J Hydrogen Energy 1998;23:355–62.

[157] Kim JK, Park IS, Kim KJ, Gawlik K. A hydrogen-compression system using porous metal hydride pellets of $LaNi_{5-x}Al_x$. Int J Hydrogen Energy 2008;33:870–7.

[158] Bhuiya MH, Lee CY, Hopkins R, Yoon H, Kim S, Park SH, et al. A high-performance dual-stage hydrogen compressor system using $Ca_{0.2}Mm_{0.8}Ni_5$ metal hydride. In: Proc ASME 2011 Conf on smart materials, adaptive structures and intelligent systems, SMASIS2011; September 18–21, 2011. Scottsdale, Arizona, USA; SMASIS2011-5120.

[159] Kim KJ, Montoya B, Razania A, Lee KH. Metal hydride compacts of improved thermal conductivity. Int J Hydrogen Energy 2001;26:609–13.

[160] Rodríguez Sánchez A, Klein HP, Groll M. Expanded graphite as heat transfer matrix in metal hydride beds. Int J Hydrogen Energy 2003;28:515–27.

[161] Klein HP, Groll M. Heat transfer characteristics of expanded graphite matrices in metal hydride beds. Int J Hydrogen Energy 2004;29:1503–11.

[162] Popeneciu G, Coldea I, Lupu D, Misan I, Ardelean O. Metal hydrides reactors with improved dynamic characteristics

for a fast cycling hydrogen compressor. J Phys Conf Ser 2009;182:012054.
[163] De Rango P, Chaise A, Fruchart D, Marty P, Miraglia S. Hydrogen storage tank. Patent US 2010/0326992 Al, 2010.
[164] Inoue S, Iba Y, Matsumura Y. Drastic enhancement of effective thermal conductivity of a metal hydride packed bed by direct synthesis of single-walled carbon nanotubes. Int J Hydrogen Energy 2012;37:1836–41.
[165] Pohlmann C, Röntzsch L, Heubner F, Weißgärber T, Kieback B. Solid-state hydrogen storage in hydralloy–graphite composites. J Power Sources 2013;231:97–105.
[166] Takeichi N, Senoha H, Yokota T, Tsuruta H, Hamada K, Takeshita HT, et al. "Hybrid hydrogen storage vessel", a novel high-pressure hydrogen storage vessel combined with hydrogen storage material. Int J Hydrogen Energy 2003;28:1121–9.
[167] Mori D, Kimura Y, Nito T, Kimbara M, Shinozawa T, Toh K, et al. Hydrogen storage container and method of occluding hydrogen. Patent application EP 1384 940 A2, 2003.
[168] Okumura M, Terui K, Ikado A, Saito Y, Shoji M, Matsushita Y, et al. Investigation of wall stress development and packing ratio distribution in the metal hydride reactor. Int J Hydrogen Energy 2012;37:6686–93.
[169] Cieslik J, Kula P, Sato R. Performance of containers with hydrogen storage alloys for hydrogen compression in heat treatment facilities. J Alloys Compds 2011;509:3972–7.
[170] Nomura K, Ishido Y, Ono S. A novel thermal engine using metal hydride. Energy Convers 1979;19:49–57.
[171] Northrup Jr CJM, Heckes AA. A hydrogen-actuated pump. J Less-Common Met 1980;74:419–26.
[172] Ergenics Corp.*. Metal hydride hydrogen compressors. http://www.ergenics.com/compression.html. * HERA USA since 2003; acquired by ERRA Inc (http://www.errainc.com) in 2009.
[173] Wade LA, Bowman Jr RC, Gilkinson DR, Sywulka PH. Development of sorbent bed assembly for a periodic 10 K solid hydrogen cryocooler. Adv Cryog Eng 1994;39:1491–8.
[174] Bard S, Wu J, Karlmann P, Cowgill P, Mirate C, Rodgriguez. Ground testing of a 10 K sorption cryocooler flight experiment (BETSCE). In: Ross Jr RG, editor. Cryocoolers, 8. New York: Plenum Press; 1995. pp. 609–21.
[175] Bowman Jr RC, Karlmann PB, Bard S. Post-flight analysis of a 10 K sorption cryocooler. Adv Cryog Eng 1998;43:1017–24.
[176] Shmalko YuF, Ivanovsky AI, Lototsky MV, Karnatsevich LV, Milenko YuYa. Cryo-hydride high-pressure hydrogen compressor. Int J Hydrogen Energy 1999;24:649–50.
[177] Vanhanen JP, Hagström MT, Lund PD. Combined hydrogen compressing and heat transforming through metal hydrides. Int J Hydrogen Energy 1999;24:441–8.
[178] Industrial Technology Research Institute. Metal hydride thermal hydrogen compression technology; http://www.itri.org.tw/eng/econtent/research/research05_02.aspx?sid=1.
[179] Golubkov AN, Grishechkin SK, Yukhimchuk AA. System for investigation of hydrogen isotopes – solid body interaction at 500 MPa. Int J Hydrogen Energy 2001;26:465–8.
[180] Laurencelle F, Dehouche Z, Morin F, Goyette J. Experimental study on a metal hydride based hydrogen compressor. J Alloys Compds 2009;475:810–6.
[181] Wang XH, Bei YY, Song XC, Fang GH, Li SQ, Chen CP, et al. Investigation on high-pressure metal hydride hydrogen compressors. Int J Hydrogen Energy 2007;32:4011–5.
[182] Cieslik J, Kula P, Filipek SM. Research on compressor utilizing hydrogen storage materials for application in heat treatment facilities. J Alloys Compds 2009;480:612–6.
[183] Popeneciu G, Almasan V, Coldea I, Lupu D, Misan I, Ardelean O. Investigation on a three-stage hydrogen thermal compressor based on metal hydrides. J Phys Conf Ser 2009;182:012053.
[184] Li H, Wang X, Dong Z, Xu L, Chen C. A study on 70 MPa metal hydride hydrogen compressor. J Alloys Compds 2010;502:503–7.
[185] Pickering L. Two stage metal hydride compressor. UK Sustainable Hydrogen Energy Consortium; http://www.uk-shec.org.uk/uk-shec/events/workshops/Lydia_Pickering.pdf.
[186] Book D. Materials for hydrogen storage & separation. In: H2FC Supergen hydrogen and fuel cell Hub meeting. Aberdeen: All-Energy, AECC; 21 May 2013. http://www.h2fcsupergen.com/wp-content/uploads/2013/06/Materials-for-Hydrogen-Storage-and-Seperation-Dr-David-Book-Birmingham.pdf.
[187] HYSTORSYS AS. Hystorsys metal hydride compressor being delivered to the HyNor Lillestrøm refuelling station in May 2013; http://www.hystorsys.no/download/Hystorsys_One-sheet_Overview.pdf.
[188] HYSTORSYS AS. The metal hydride (MH) compressor. Opening of the HL innovation zone http://www.hystorsys.no/download/2013-05-28_HYSTORSYS_HL_InnovationZone_Opening.pdf; May 28, 2013.
[189] Powell JR, Salzano FJ. Hydride compressor. Patent US 4085590, 1978.
[190] Popovich VA, Makarov AA, Solovey VV, Postoyuk YI. Method of operation of a thermal sorption compressor. Author's Certificate SU 1326850 A1; 1987.
[191] Sywulka PH. Regenerative sorption compressor assembly. Patent US 5419156 A, 1995.
[192] Critoph RE, Thorpe R. Thermal compressive device. Patent US 5845507, 1998.
[193] Bowman Jr R, Prina M, Schmelzel ME, Lindensmith CA, Barber DS, Bhandari P, et al. Performance, reliability, and life issues for components of the Planck sorption cooler. Adv Cryog Eng 2002;47:1260–7.
[194] Mueller WM, Blackledge JP, Libowitz GG. Metal hydrides. New York: Academic Press; 1968.
[195] Beavis LC. Characteristics of some binary transitional metal hydrides. J Less Common Met 1969;19:315–28.
[196] Bowman Jr RC, Carlson RS, DeSando RJ. Characterization of metal tritides for the transport, storage, and disposal of tritium. In: Proc. 24th Conf. remote systems Technol.; 1976. pp. 62–8.
[197] Nasise JE. Performance and improvements of the tritium handling facility at the Los Alamos Scientific Laboratory. In: Wittenberg LJ, editor. Proceedings of tritium technology in fission, fusion and isotopic applications; 1980. pp. 347–59. US DOE Document CONF-800427.
[198] Ortman MS, Hueng LK, Nobile A, Rabun III RL. Tritium processing at the Savannah River site: present and future. J Vac Sci Technol A 1990;8:2881–9.
[199] Kherani NP, Shmayda WT. Gas handling systems using titanium-sponge and uranium bulk getters. Fusion Technol 1985;8:2399–406.
[200] Nobile Jr A. Experience using metal hydrides for processing tritium. Fusion Technol 1991;20:186–99.
[201] Motyka T. The replacement tritium facility. Fusion Technol 1992;21:247–52. /195/.
[202] Heung LK. Developments in tritium storage and transportation at the Savannah River Site. Trans Fusion Technol 1995;27:85–90.
[203] Motyka T. Private communication to RC Bowman; 2013.
[204] Van Mal HH, Mijnheer A. Hydrogen refrigerator for the 20 K region with a LaNis-hydride thermal absorption compressor for hydrogen. In: Proceedings 4th international cryogenic engineering conference. Guildford, UK: IPC Science and Technology Press; 1972. pp. 122–5.

[205] Van Mal HH, Miedema AR. Some applications of $LaNi_5$-type hydrides. In: Andresen AF, Maeland AJ, editors. Hydrides for energy storage, Proc. Int. Symp. Geilo, Norway. New York: Pergamon Press; 1978. pp. 251–60.
[206] Jones JA, Golben PM. Design, life testing, and future designs of cryogenic hydride refrigeration systems. Cryogenics 1985;25:212–9.
[207] Karperos K. Operating characteristics of a hydrogen sorption refrigerator part 1: experiment design and results. In: Green G, Patton G, Knox M, editors. Proc 4th international cryocoolers conference. Annapolis, MD: David Taylor Naval Ship Research & Development Center; 1987. pp. 1–16. http://www.dtic.mil/dtic/tr/fulltext/u2/a211760.pdf.
[208] Feng Z, Deyou B, Lijun J, Liang Z, Xiaoyu Y, Yiming Z. Metal hydride compressor and its application in cryogenic technology. J Alloys Compds 1995;231:907–9.
[209] Tauber JA, Mandolesi N, Puget J-L, Banos T, Bersanelli M, Bowman R, et al. Planck pre-launch status: the Planck Mission. Astron Astrophys 2010;520:A1.
[210] Mandolesi N, Bersanelli M, Butler RC, Artal E, Baccigalupi C, Bowman RC, et al. Planck pre-launch status: the Planck-LFI programme. Astron Astrophys 2010;520:A3.
[211] Ade PAR, Aghanim N, Arnaud M, Ashdown M, Aumont J, Bowman B, et al. Planck early results. II. The thermal performance of Planck. Astron Astrophys 2011;536:A2.
[212] Solovey AI, Frolov VP. Metal hydride heat pump for watering systems. Int J Hydrogen Energy 2001;26:707–9.
[213] Rajendra Prasad UA, Prakash Maiya M, Srinivasa Murthy S. Parametric studies on a heat operated metal hydride based water pumping system. Int J Hydrogen Energy 2003;28:429–36.
[214] Debashis Das, Ram Gopal M. Studies on a metal hydride based solar water pump. Int J Hydrogen Energy 2004;29:103–12.
[215] Hydride heat engine prototype by Ergenics. http://www.youtube.com/watch?v=d0bt1RGJsJY.
[216] Rusanov AV, Solovey VV, Goloschapov VN. Thermo-and-gas dynamic performances of turbine expansion engine for hydrogen liquefier with thermal sorption compressor. Bull Natl Tech Univ "KhPI", Ser Power Therm Process Apparatus 2012;8:76–81.
[217] Wang Y, Zheng L, Yang F, Meng X, Zhang Z. Performance comparison and analysis of typical energy conversion cycles. In: 2011 international conference on computer distributed control and intelligent environmental monitoring. IEEE; 2011. pp. 1603–6.
[218] Sasaki T, Kawashima T, Aoyama H, Ogawa T, Ifukube T. Development of an actuator using a metal hydride and its application to a lifter for the disabled. Adv Robot 1987;2:277–86.
[219] Wakisaka Y, Muro M, Kabutomori T, Takeda H, Ifukube. Investigation of applicaions of a large-output metal hydride (MH) actuator for use in rehabilitation equipment. J Robot Soc Jpn 1997;15:1060–7.
[220] Itoh H, Kautomori T, Takeda H. Other applications (actuator, hydrogen purification, and isotope separation). In: Ohta T, editor. Energy carriers and conversion systems, vol. 2. Encyclopedia of Life Support Systems (EOLSS); 2013. http://www.eolss.net/ebooklib.
[221] Kwon TK, Jeon WS, Pang DY, Choi KH, Kim NG, Lee SC. Development of SMH actuator system using hydrogen-absorbing alloy. In: ICCAS2005, June 2-5, KINTEX, Gyeonggi-Do, Korea.
[222] Lloyd GM, Kim KJ. Smart hydrogen/metal hydride actuator. Int J Hydrogen Energy 2007;32:247–55.
[223] Vanderhoff A, Kim KJ. Experimental study of a metal hydride driven braided artificial pneumatic muscle. Smart Mater Struct 2009;18. 125014 (10pp).
[224] Sato M, Hosono M, Yamashita K, Nakajima S, Ino S. Solar or surplus heat-driven actuators using metal hydride alloys. Sensors Actuators 2011;B156:108–13.
[225] Siler S. Hydrogen filling stations are still rare http://www.caranddriver.com/features/pump-it-up-we-refuel-a-hydrogen-fuel-cell-vehicle; November 2008.
[226] Weinert JX, Shaojun L, Ogden JM, Jianxin M. Hydrogen refueling station costs in Shanghai. Int J Hydrogen Energy 2007;32:4089–100.
[227] Ovshinsky SR, Young RT, Huang B, Bavarian F, Nemanich G. Hydrogen infrastructure, combined bulk hydrogen storage/single stage metal hydride hydrogen compressor therefore and alloys for use therein. Patent US 6591616 B2, 2003.
[228] HyNor Lillestrøm: making hydrogen green; http://hynor-lillestrom.no/english/content_1/textwithimage_c4a41059-6c46-4ccf-87a3-57febeefd146/1300138907972/hynor_flyer_ferdig_low.pdf.
[229] HyNor Lillestrøm fuelling station using P + E hydrogen purifier. Fuel Cells Bull; March 2013:6–7.